Overnutrition directly impairs thyroid hormone biosynthesis and utilization, causing hypothyroidism, despite remarkable thyroidal adaptations

Jessica Rampy,[1,2] Alejandra Paola Torres-Manzo,[2] Kendra Hoffsmith,[2] Matthew A. Loberg,[3] Quanhu Sheng,[4] Federico Salas-Lucia,[5] Antonio C. Bianco,[5*] Rafael Arrojo e Drigo,[2,6] Huiying Wang,[3] Vivian L. Weiss,[3] and Nancy Carrasco[2]

1. Department of Cellular & Molecular Physiology, Yale University, New Haven, CT
2. Department of Molecular Physiology & Biophysics, Vanderbilt University, Nashville, TN
3. Department of Pathology, Microbiology, & Immunology, Vanderbilt University Medical Center, Nashville, TN
4. Department of Biostatistics, Vanderbilt University Medical Center, Nashville, TN
5. Department of Medicine, The University of Chicago, Chicago, IL
6. Center for Computational Systems Biology, Vanderbilt University, Nashville, TN

*Current affiliation: Division of Endocrinology, University of Texas Medical Branch, Galveston, TX

Corresponding author:

Nancy Carrasco
2215 Garland Avenue
Light Hall 707
Nashville, TN 37232-0615, USA
nancy.carrasco@vanderbilt.edu

The authors have declared that no conflict of interest exists.

Abstract:

Thyroid hormones (THs: T_3 and T_4) are key regulators of metabolic rate and nutrient metabolism. They are controlled centrally and peripherally in a coordinated manner to elegantly match T_3-mediated energy expenditure (EE) to energy availability. Hypothyroidism reduces EE and has long been blamed for obesity; however, emerging evidence suggests that, instead, obesity may drive thyroid dysfunction. Thus, we used a mouse model of diet-induced obesity to determine its direct effects on thyroid histopathology and function, deiodinase activity, and T_3 action. Strikingly, overnutrition induced hypothyroidism within 3 weeks. Levels of thyroidal THs and their precursor protein thyroglobulin decreased, and ER stress was induced, indicating that thyroid function was directly impaired. We also observed pronounced morphological and vascular expansion in the thyroid. Overnutrition additionally suppressed T_4 activation, rendering the mice resistant to T_4 and reducing EE. Our findings collectively show that overnutrition deals a double strike to TH biosynthesis and action, despite large efforts to adapt—but, fortunately, thyroid dysfunction in mice can be reversed by weight loss. In humans, BMI correlated with thyroidal vascularization, importantly demonstrating initial translatability. These studies lay the groundwork for novel obesity therapies that tackle hypothyroidism—which are much-needed, as no current obesity treatment works for everyone.

Introduction:

The thyroid hormones (THs: T_3 and T_4) are required for physiological regulation of energy homeostasis, carbohydrate and lipid metabolism, thermogenesis, and cellular metabolism (1). Thyroid function is directly regulated by thyroid stimulating hormone (TSH), and THs suppress TSH synthesis and release by the pituitary. This negative feedback loop is part of the hypothalamic–pituitary–thyroid (HPT) axis. When TH levels are low, TSH levels rise to stimulate every major step of TH biosynthesis (2). Thyrocytes synthesize and properly fold the ~660 kDa protein dimer thyroglobulin (TG) and secrete it into the follicular colloid. Iodide (I^-) is actively transported by the Na^+/I^- symporter (NIS) from the blood into the thyrocytes (3–5) and eventually gets incorporated onto tyrosyl residues of TG in the colloid. Finally, iodinated TG is endocytosed back into the thyrocytes, where the THs are cleaved from TG and released into the blood.

It has been known for over a century that THs are potent stimulators of energy expenditure (EE) and that hypothyroidism reduces EE (6). In fact, basal metabolic rate (BMR) is directly correlated with serum T_4 levels (7). Hypothyroidism, even when mild, also causes other metabolic dysfunctions, including hyperlipidemia, cardiovascular disease, and metabolic dysfunction–associated steatotic liver disease (MASLD) (8–12). Whether hypothyroidism causes weight gain is intensely debated: several studies report an inverse association between thyroid function and BMI (13–15), whereas others demonstrate that treatment of hypothyroidism results in only modest weight loss, attributable to appropriate fluid loss in some cases (16, 17). Even so, obesity is, on the whole, associated with normal or high TSH levels and normal or low free T_4 levels (16), as well as with an increased prevalence of hypothyroidism (18). Due to THs' potent effects on EE, it has long been postulated that obesity is secondary to hypothyroidism when these disorders coincide. However, the lack of compelling data linking primary hypothyroidism to weight gain calls this assumption into question. Rather, mounting evidence suggests that obesity can induce thyroid dysfunction, in line with its deleterious effects on many other hormonal systems (16). For instance, obesity is associated with greater thyroid volume, attributable to elevated TSH (19), and with a hypoechogenic ultrasound pattern in the thyroid, a diagnostic sign of reduced thyroid function (20–22). Moreover, a meta-analysis of bariatric patients revealed that preoperative TSH

and serum T_3:T_4 were high (23). All these phenomena are routinely interpreted as evidence of inadequate thyroid function in various forms of hypothyroidism and are improved by weight loss (20, 23–28).

Some argue that elevated TSH in obese subjects is a physiological adjustment to increase THs and EE to combat positive energy balance. However, studies show that elevation of serum T_3 in response to overfeeding is a homeostatic mechanism for increasing EE that does not require increased TSH stimulation of the thyroid in lean subjects (29–31). Mechanistically, this pattern is accomplished by increased peripheral T_4-to-T_3 conversion by deiodinases (32). T_4 is converted to T_3 by deiodinase 1 (D1) and deiodinase 2 (D2), which are highly expressed in liver and brown adipose tissue (BAT), respectively (33). T_4 can also be inactivated by deiodinase 3 (D3), which is abundant in the brain. Whereas the thyroid secretes mostly the prohormone T_4 (34), D2 is the body's main producer of T_3, the active hormone, underscoring the importance of peripheral mechanisms to regulate serum TH levels. A recent meta-analysis of overfeeding in lean subjects concurred that overnutrition increased T_3—and consequently T_3:T_4—in most studies, but not a single study found a change in TSH (35). In contrast, the co-occurrence of elevated TSH with increased T_3:T_4 in obese subjects, along with the other thyroid symptoms described, make a strong case for obesity-induced thyroid dysfunction, not simply physiological adaptation. Data regarding how obese subjects respond to experimental overfeeding is sparse, underpowered, and conflicting (36–38). Furthermore, the effect of obesity on deiodinase activity is not yet well understood but could dampen the body's ability to upregulate EE.

To further elucidate the effects of obesity on thyroid function and TH action, we used a mouse model of overnutrition to interrogate its effects on systemic TH levels and thyroid histology and function, with a particular emphasis on identifying biochemical mechanisms by which short-term overnutrition may impair thyrocyte activity. Our results indicate that overnutrition directly impairs thyroid function while also triggering remarkable, albeit insufficient, compensatory mechanisms aimed at increasing TH biosynthesis within the thyroid—a phenotype mostly reversed by weight loss. We also found that overnutrition modulates deiodinase activity, resulting in reduced whole-body T_4-to-T_3 conversion rate and EE. Importantly, we discovered similar histological changes in human thyroids associated with high BMI. These findings support the hypothesis that thyroid dysfunction may be secondary to obesity in many patients, and highlight the key role that TH action plays in increasing metabolic rate. Furthermore, TH action could be harnessed to promote weight loss that could ultimately repair obesity-related thyroid damage.

Results:

Overnutrition induces hypothyroidism and goiter

Male C57Bl/6J mice were placed on a high-fat food plus sucrose water diet (HF+SD) for a short period of time (6 weeks; **Figure 1A**). These mice consumed more calories than control mice and increased their BW and fat mass (**Figure 1, B–D**). Whereas serum T_3 levels were maintained, serum T_4 decreased and TSH increased within 3 weeks, the latter worsening in a time-dependent manner (**Figure 1, E–G**). The HF+SD-fed mice also progressively developed goiter within 3 weeks (**Figure 1H**). Goiter is a classic symptom of hypothyroidism resulting from a sustained elevation in TSH levels, which is well known to have mitogenic effects (2). These results indicate that overnutrition induces mild hypothyroidism in this mouse model. The diet-induced hypothyroidism was not due to I^- deficiency, as I^- excretion was not different between groups at any timepoint (**Supplemental Figure 1**). HF+SD-fed female mice exhibited a similar, albeit milder,

systemic thyroid status, whereas their goiters were as pronounced as those of their male counterparts. Interestingly, their BW increase was only a trend, and their fat mass was unchanged relative to that of the controls (**Supplemental Figure 2**). Thus, the diet-induced hypothyroid phenotype, particularly its goiter component, is reasonably robust across the two sexes.

Overnutrition reduces T_4-to-T_3 conversion and EE by impairing D2 activity

To investigate TH metabolism, we measured deiodination rates in tissues from male mice on the HF+SD for 6 weeks. There was no difference in D3 activity in either the hippocampus or the cortex (**Figure 2A**), suggesting that D3-mediated inactivation of T_4 is not a major contributor to diet-induced hypothyroidism. In contrast, liver D1 activity increased (**Figure 2B**). However, the effect of high liver D1 on serum T_4 levels is difficult to interpret, since D1 has a comparatively poor affinity for T_4 and catalyzes activating and deactivating deiodination of T_4 at similar rates. Though it contributes minorly to the serum T_3 pool, its primary function is to recycle I^- by removing it from TH degradation products (39, 40). Even so, it is possible that this increase in D1 activity lowers serum T_4 levels. Finally, BAT D2 activity tended to be lower in the HF+SD-fed mice than in the control mice (**Figure 2C**), consistent with a similar trend in its protein expression (**Supplemental Figure 3, A and B**). This decrease in D2 activity would be expected to preserve serum T_4 levels rather than deplete them, indicating that D2 action, at least in adipose tissue, is not a major contributor to diet-induced hypothyroidism. Similar results for the three deiodinases were obtained in female mice (**Supplemental Figure 3, C–E**).

To determine the combined effects of these overnutrition-induced changes in deiodinase activity on whole-body TH utilization, we performed a metabolic cage experiment quantitating the energetic response to TH administration (**Figure 2D**). Not surprisingly, all the mice receiving exogenous THs increased their EE (**Figure 2E**). The diet groups responded similarly to T_3, suggesting that TH degradation rates are unchanged by the HF+SD, consistent with our D3 activity assay results. However, the HF+SD-fed mice exhibited a reduced response to T_4 than did the lean mice, though their serum T_4 and TSH levels were not different (**Supplemental Figure 4, A and B**). Furthermore, differences in EE were not due to differences in locomotor activity (**Supplemental Figure 4C**). This outcome strongly suggests that overnutrition impairs whole-body conversion of T_4 to T_3 and that this impairment has a functional effect—overall EE is reduced. This result is most simply explained by decreased D2 activity—likely in various tissues, given that the differences we observed in BAT were admittedly small. Thus, it is clear that the observed increase in liver D1 activity does not compensate for decreased D2 activity systemically, and the ultimate effect of overnutrition on peripheral TH metabolism is decreased activation of T_4 and a slowed metabolic rate.

Overnutrition induces hypothyroidism by directly impairing thyroid function

The reduced serum T_4 levels brought about by overnutrition could result from reduced TH biosynthesis. Thus, we characterized TH biosynthesis at various study endpoints directly by measuring the TH content in proteolytically digested thyroid homogenates, since most TH in the thyroid is covalently bound to TG. Strikingly, the thyroidal T_4 content of male mice decreased after just 1.5 weeks of HF+SD feeding, and the percent reduction appears to progressively worsen (**Figure 3A**). Thyroidal T_3 biosynthesis in these mice remained unchanged during their first 3 weeks on the HF+SD but began to decline by 6 weeks—a decline that reached statistical significance by 12 weeks (**Figure 3B**). We also observed a robust increase in the T_3:T_4 ratio in response to overnutrition at all timepoints (**Figure 3C**), a well characterized response to TSH

stimulation and thyroid disease (41). Despite continued thyroid growth after 12 weeks of the HF+SD (**Figure 3D**), the efficiency of TH biosynthesis (total TH/protein content) was notably lower in the HF+SD group, indicating that overnutrition induces mild hypothyroidism by directly impairing thyroid function.

Overnutrition leads to pronounced histological changes in the thyroid

To identify potential mechanisms by which overnutrition directly impairs thyroid function, we characterized its effect on the histopathology of the thyroid. Healthy thyrocytes from CD-fed mice are thin and flat, with a high nuclear-to-cytoplasmic (N/C) ratio (**Figure 4A**). The HF+SD greatly expanded the thyrocytes' cytoplasmic volume (thyroids with high N/C ratio: HF+SD = 0% vs. CD = 100%) and granularity, indicating greater organelle content (**Figure 4, B and C**). These results are consistent with the classic mitogenic effects of high TSH levels (2, 42), suggesting that TSH signaling remains at least partially intact. Furthermore, the thyroids from the HF+SD mice displayed larger interfollicular vascular/lymphatic space (**Figure 4D**). Since no immune cell invasion was observed, we performed immunohistochemical staining with the vascular marker CD31, revealing that overnutrition increased both the circumferential coverage of thyroid follicles by microcapillaries and their dilatation (**Figure 4, E–H**). We observed similar results in males after 3 weeks and in females after 6 weeks (**Supplemental Figure 5**). The overall picture that emerges from these histological findings is one in which the thyroid gland adapts to overnutrition by increasing its TH biosynthesis and delivery capacity. Although this state is consistent with the effects of TSH stimulation, it does not explain the impaired thyroid function we observed.

Overnutrition induces thyroidal ER stress, limits TG synthesis, and alters mitochondria

Next, we investigated the morphological adaptation more deeply by electron microscopy (EM). The hypertrophy of the thyrocytes, their increased granularity, and the increased and dilated follicular vasculature of the HF+SD mice were even more apparent at a higher magnification (**Figure 5, A and B**). We employed deep learning models to quantitate several morphological parameters, achieving 80–95% accuracy (**Supplemental Figure 6A**). As was already apparent, 6 weeks of the HF+SD caused thyrocyte hypertrophy and increased granularity mediated mostly by expansion of the ER and increased mitochondrial density (**Figure 5, C and D; Supplemental Figure 6, B–E**). However, only complex IV was upregulated, whereas other complexes were expressed at the same levels as in control mice. Interestingly, though, the ATP synthase—complex V—was downregulated (**Supplemental Figure 7**), suggesting that overnutrition may induce some degree of mitochondrial dysfunction. If production of ATP is impaired, its availability may be a factor limiting TH biosynthesis, a possibility that should be investigated in further studies.

Thyrocytes are secretory cells, producing large amounts of TG for TH biosynthesis. TG synthesis requires considerable energy and resources, as it involves the translation and folding of the ~660 kDa dimer in the ER, post-translational modifications in the ER and Golgi, and vesicular secretion into the colloid (41). It is thus no surprise that thyrocytes contain much ER and that stimulation by TSH causes the ER and mitochondrial compartments to expand. However, the thyrocytes from the HF+SD mice exhibited more ER bloating than did controls, suggesting ER stress (**Figure 5, A and B**). We measured several markers of ER stress, revealing that overnutrition increased thyroidal expression of molecular chaperone BiP and phosphorylation of translation initiation factor eIF2α, whereas the expression of transcription factor CHOP remained unchanged (**Figure 5, E and F; Supplemental Figure 8A**). These results indicate ER stress severe enough to arrest global translation but not induce apoptosis (43, 44). Even so, the halting of translation could have

a deleterious effect on the function of thyrocytes, as it should limit the synthesis of TG. Indeed, TG expression was decreased (**Figure 5, E and G; Supplemental Figure 8B**), even though *Tg* mRNA transcript levels were slightly elevated in the thyroids of HF+SD mice (**Table 1**). In addition, the expression of two molecular chaperones critical for proper TG folding—PDI and Ero1-Lα—was significantly elevated (**Figure 5, E and H; Supplemental Figure 8, C and D**). Thus, although the EM data are consistent with the picture of a thyroid gland adapting to increase its TH biosynthesis and delivery capacity, ER stress impairs TG biosynthesis and ultimately limits TH biosynthesis, resulting in thyroid dysfunction.

Since lipotoxicity induces ER stress (45–47), we measured total triglycerides and an array of sphingolipid species in thyroid tissue, revealing mostly similar and even decreased lipid levels in the HF+SD group (**Supplemental Figure 9**). Thus, ceramide accumulation does not account for the thyrocyte dysfunction we observed. In fact, increased dihydroxy-sphingosine without an increase in downstream ceramides, as we observed, can itself result from ER stress (48). Only EM was sensitive enough to reveal lipid deposition (**Figure 5B**), and quantitative analysis showed a shift in the percentage of thyrocytes containing one or more lipid droplets (LDs) in the HF+SD group (1 LD: HF+SD = 26.2% vs. CD = 9.5%; >1 LD: HF+SD = 26.2% vs. CD = 4.8%; n = 42 cells/group). However, almost half the HF+SD thyrocytes did not contain any LDs, and it is unclear whether the small number of LDs observed could induce such marked ER stress and thyrocyte dysfunction.

High TSH signaling appears unimpaired and likely drives the increased thyroidal vascularization by upregulating adrenomedullin 2 (ADM2) expression in thyrocytes

We performed bulk RNA-sequencing of mouse thyroid tissue to investigate other possible mechanisms underlying our phenotype. Six weeks of the HF+SD induced differential expression of over 6,000 genes (**Figure 6A**). Gene set enrichment analysis (GSEA) using GO annotations yielded many top upregulated gene sets related to cellular proliferation (**Table 2**), consistent with the mitogenic effects of TSH and our histological data (**Figure 1, G and H; Figure 4**). The most downregulated gene sets were related to mitochondrial structure and function and translation, in line with our previous findings suggesting changes in mitochondria and ER stress (**Supplemental Figures 6 and 7; Figure 5**). Additional downregulated translation-related gene sets appeared after 3 weeks of overnutrition, suggesting that overnutrition may induce ER stress quite rapidly in the thyroid (**Supplemental Table 1**).

Another hypothesis is that perhaps the modest ectopic lipid deposition observed was enough to induce resistance to the elevated TSH, akin to overnutrition-induced insulin and leptin resistance (16). However, NIS protein expression was highly upregulated in both male and female mice on the HF+SD (**Figure 6B; Supplemental Figure 10**), and TSH-responsive genes were expressed at higher levels in the HF+SD group (**Table 1**). Moreover, two of the top upregulated individual genes that we identified were *Adm2*, a vasodilator and angiogenic factor known to respond to TSH stimulation (49–52), and its receptor modulator *Ramp3* (**Figure 6A**). Immunohistochemistry revealed that overnutrition increased ADM2 expression in thyrocytes (**Figure 6, C and D**). Thus, we conclude that TSH signaling is increased by overnutrition, not blocked. We also propose that the HF+SD-fed mice exhibit an adaptive mechanism whereby their elevated TSH levels upregulate thyrocyte ADM2 expression, which drives vascularization in a paracrine signaling fashion. Ultimately, this process supports thyroid growth and delivery of nutrients needed for TH biosynthesis, but unfortunately, this compensatory mechanism does not rescue thyroid function.

Thyroidal changes caused by overnutrition are mostly reversible

An important subsequent question is whether the damage inflicted by overnutrition is reversible. To answer this question, we placed male mice on the HF+SD for 6 weeks and then returned them to the CD for another 6 weeks (the reversed group: REV). The REV mice gained weight and then rapidly lost it, matching the BW and fat masses of the control mice by the end of the study (**Figure 7, A and B**), and maintained a normal energy balance during the study's final weeks (**Supplemental Figure 11, A and B**), suggesting no modulation of THs by energy balance during that time. Hearteningly, most of the functional damage to the thyroid induced by overnutrition appears to be reversible by weight loss. Serum T_3 levels remained unchanged, and T_4 and TSH levels returned to normal (**Figure 7, C–E**). The goiter was mostly rescued, since the thyroids of the REV mice were only ~50% larger than those of the controls (**Figure 7F**), in contrast to those of the mice fed the HF+SD for 12 weeks, which grew ~250% as large (**Figure 3D**). Even so, the thyroidal T_4 and T_3 levels and their ratio returned to normal, as did the histology (**Figure 7, G–I; Supplemental Figure 11, C–F**), consistent with the normalization of TSH levels. Furthermore, we found no indication of ER stress, TG and NIS protein levels returned to normal, and the levels of TG's folding chaperones decreased (**Figure 7J; Supplemental Figure 12**). These findings strongly suggest that thyroid dysfunction can be reversed by dietary intervention and weight loss in mice.

BMI may affect thyroid function directly in humans

To ascertain the translatability of our findings, we performed histologic analysis of surgically resected human thyroid tissue from patients with multinodular goiter (MNG; **Figure 8, A–F**). Importantly, we found that patients with obesity exhibited increased vascular/lymphatic space, and CD31 staining revealed a stepwise increase in vascularization (**Figure 8, G–I**). Spearman correlation tests between each of these scores and the individual patients' BMIs revealed that in each case, the score was significantly positively correlated with BMI (**Supplemental Table 2**). RNA-sequencing results from a subset of these patients showed that *Adm2* did not correlate with BMI, but its closely related family member adrenomedullin (*Adm*) was positively correlated with BMI (**Supplemental Figure 13**). ADM is also a vasodilator and angiogenic factor and shares a receptor subunit with ADM2 (51). These findings indicate that some of the thyroidal responses to overnutrition that we have observed in mice have close counterparts in humans, suggesting that obesity may affect thyroid function directly in humans. These results also bolster the hypothesis that obesity drives thyroid dysfunction, rather than the converse, in line with the other emerging evidence mentioned previously.

Discussion:

The systemic thyroid status induced by a short period of overnutrition in mice—i.e., normal serum T_3 levels, but decreased serum T_4 levels, and high TSH levels (**Figure 1, E–G**)—is also characteristic of the early stages of hypothyroidism in humans, when small decreases in serum T_4 levels stimulate TSH secretion, while other homeostatic mechanisms preserve serum T_3 levels (53). Since the decreased serum T_4 levels in our mice are accompanied by increased TSH levels, we conclude that their thyroid status is truly less than adequate. Female mice were resistant to obesity despite increased caloric intake, consistent with well-documented sexual dimorphisms (54). Notably, however, these mice exhibited diet-induced hypothyroidism (**Supplemental Figure 2**), suggesting that their thyroid dysfunction is attributable at least in part to their diet, rather than to increased fat mass, since the female mice do not expand their adipose tissue. In line with this,

overfeeding of lean men with various macronutrient ratios had differing effects on serum T_3 levels and EE (29). More work needs to be done to distinguish the effects of dietary composition from those of obesity and to determine how they are affected by sex.

We identified remarkable compensatory mechanisms that are induced by overnutrition in both sexes, which are attributable to the elevated TSH levels and would be expected to promote greater TH biosynthesis. Thyrocyte hypertrophy and hyperplasia, i.e. goiter, are classic effects of TSH documented for over a century (2, 42). We are, to our knowledge, the first to report quantitative organelle expansion in thyrocytes during overnutrition (**Figure 5 and Supplemental Figure 6**). Given the requirement for TG and ATP for TH synthesis, it seems unlikely that bigger thyrocytes could synthesize more TH without more ER and mitochondria. Although the underlying mechanism requires further investigation, we believe the organelle expansion we have observed is consistent with the mitogenic effects of TSH. Increased vascularization was also described in goitrous thyroids more than a century ago, in cases of I^- deficiency disorder (IDD) (42). Nagasaki *et al* reported that I^--deficient rats exhibited high levels of thyrocyte ADM2 and that TSH stimulates ADM2 secretion *in vitro* (52). To our knowledge, however, we are the first to report that overnutrition increases vascularization in normal I^--sufficient thyroid tissue, accompanied by marked elevation in thyrocyte ADM2 (**Figure 6**). Thus, while we cannot rule out other possible mechanisms, it is reasonable to conclude that the common cause of increased thyroidal vascularization in IDD and overnutrition is elevated TSH levels.

Despite these thyroidal adaptations triggered by TSH, systemic overnutrition-induced hypothyroidism persists due to direct impairment of thyroid function. We found, for the first time, that overnutrition decreases the T_4 content of the thyroid within just 10 days (**Figure 3**). Because thyroid growth does not outpace declines in thyroidal T_4 content, net T_4 production from the thyroid gland appears to be reduced by overnutrition. Net T_3 output from the thyroid may be higher than that of control mice, consistent with the maintenance of serum T_3 levels despite falling T_4 levels, whereas thyroidal T_3 eventually declines when normalized to protein. The T_3:T_4 ratio in the thyroid increases dramatically in overfed mice, a clear indication of preferential T_3 synthesis, an adaptive mechanism for preserving serum T_3 levels at the expense of the prohormone T_4 that has been well documented in other contexts involving enhanced TSH stimulation, including IDD (28, 41). TSH promotes preferential T_3 synthesis by increasing *de novo* T_3 synthesis on TG (55) and thyroidal T_4-to-T_3 conversion by D1 (56, 57). In our model, TG protein levels are decreased (**Figure 5G**) even while thyroidal T_3 levels are maintained, suggesting that perhaps the T_3 content on TG is increased. We also observed a 4-fold increase in *Dio1* expression in HF+SD thyroids (**Table 1**). It is likely that these mechanisms are at play in our model of overnutrition-induced hypothyroidism, though we cannot completely exclude other possible mechanisms.

Despite preferential T_3 synthesis, overall TH biosynthesis is impaired in our mouse model of overnutrition, and we investigated several possible mechanisms to explain this thyrocyte dysfunction. Secretory cells, including thyrocytes, are particularly sensitive to ER stress, because whereas slowed translation during ER stress is meant to restore proteostasis and prevent apoptosis, it can be detrimental to secretory function (58, 59). Indeed, we found that HF+SD-fed males exhibit ER bloating and increased expression of ER stress markers, including phosphorylated eIF2α, alongside reduced TG levels (**Figure 5**). Few studies have been done on the morphological and biochemical effects of overfeeding on the thyroid, but our results are consistent with those of previous studies carried out in rats (60–62). To our knowledge, just one study of overnutrition's effects on mouse thyroid function has been previously published (63). All

these previous studies attributed diet-induced thyroid dysfunction to lipotoxicity, although only two measured thyroid lipids. Surprisingly, we did not find compelling evidence for ectopic lipid deposition (**Supplemental Figure 9**). We posit that the rapid production of new membranes to sustain cellular and organellar growth outpaces accumulation of sphingolipids, or that ER stress is limiting ceramide synthesis (48). It is not known whether the small number of LDs we observed would be deleterious for thyrocytes, but lipid deposition has been observed in thyroids resected from some obese patients (63, 64), warranting further investigation. Another possible mechanism for thyrocyte dysfunction is the accumulation of misfolded proteins, including TG, during the prolonged TSH stimulation of thyroid protein synthesis. Many *Tg* mutations result in ER stress and congenital hypothyroidism, some of which resemble the overnutrition-induced ER stress that we and others have observed (59, 65). Additionally, our findings suggest that mitochondrial function may be altered (**Supplemental Figures 6 and 7**), though information on mitochondrial regulation in thyrocytes is admittedly sparse.

We have also provided evidence that overnutrition decreases the whole-body T_4-to-T_3 conversion rate, leading to resistance to T_4 and reduced EE (**Figure 2E**). These effects are likely mediated by reduced peripheral D2 activity, possibly in BAT and likely in other D2-expressing metabolic tissues. Any increase in serum T_3 levels mediated by the increased liver D1 activity is outweighed by decreased production of T_3 by D2. Moreover, we found no difference in the energetic response to exogenous T_3 between diet groups, indicating that whole-body T_3 inactivation rates (either by D3 or D1) are not changed by overnutrition. Because the affinity of D3 and D1 for T_4 is less than or equal to their affinity for T_3 (40), it is unlikely that direct inactivation of the exogenous T_4 by D3 or D1 explains our findings. Thus, we conclude that the effects of overnutrition on the body's energetic response to THs are mediated by reduced activation of T_4 by D2 rather than by increased deactivation of T_4. These findings prompt important questions regarding tissue-specific T_3 signaling, since both ectopic D3 activation as well as low D2 activity and T_4 substrate availability could cause local hypothyroidism more severe than the systemic hypothyroidism.

Our finding that decreased D2 activity correlates with decreased EE agrees with the results of previous studies showing that D2KO mice are more susceptible to weight gain, insulin resistance, and cold intolerance (66–68). D2 expression and activity are also inversely correlated with obesity and insulin resistance in humans, in whom D2 is expressed in skeletal muscle, a major contributor to thermogenesis and BMR (69–72). Decreased D2 activity clearly causes metabolic perturbations, but our study showed the converse, pointing to a possible vicious cycle. Because D2 has positive effects on EE, the strategy of promoting endogenous D2 activity to treat obesity has garnered a great deal of interest: this is an attractive approach to enhancing local T_3 signaling in metabolic tissues while avoiding the harm of systemic hyperthyroidism (73). Several groups have shown that cold exposure recruits BAT activity and increases EE in lean and obese subjects, reducing fat mass in some (74, 75). Other groups have demonstrated that pharmacological induction of D2 with bile acids protects mice from diet-induced obesity and increases EE in humans (76, 77). Conversely, studies showing that weight loss itself can improve BAT activity and that obese subjects exhibit reduced BAT recruitment during cold exposure support the hypothesis that obesity impairs D2 activity (78–80). In line with this, our findings suggest that the dampening of T_3 generation by impaired D2 activity, including in BAT, may be an additional pathology related to and exacerbating obesity, lending further plausibility to the notion that D2 activity should be rectified and ideally enhanced to combat obesity. This promising therapeutic approach calls for deeper investigation in the midst of the ever-worsening obesity epidemic, especially given that not all patients respond to GLP-1R agonists (81).

The finding that obesity impairs thyroid function and T_4-to-T_3 conversion concurrently is extremely important, since these regulatory processes normally compensate for each other. Primary hypothyroidism is successfully treated with T_4 monotherapy in most patients, due to the increased production of T_3 by D2 (82–84). Moreover, mice with defects in deiodinases exhibit normal serum T_3 levels due to increased TH biosynthesis (85, 86). Our findings in mice, however, are consistent with the hypothesis that diet-induced obesity delivers a double blow to TH action by impairing both thyroid function and peripheral D2 activity, likely limiting compensation. The impairment of T_4 utilization by obesity provides a reasonable explanation for why treating obese subjects with T_4 does not consistently cause them to lose weight (87). Only supraphysiological doses of TH cause weight loss, but they cannot be administered safely (73). T_3 mimetics, however, bypass D2, and T_3 therapies targeted to the liver have been successful (88), most notably a recently FDA-approved TRβ agonist effective against MASLD (89). Additionally, T_3 delivery targeted to adipose tissue decreased BW and improved metabolic function in several mouse models of diet-induced obesity without major side effects (90). Clearly, enhancing T_3 signaling is a promising approach that should be pursued further, particularly because peripheral T_4-to-T_3 conversion decreases during calorie deficit to conserve energy in lean and obese subjects (91–93), explaining, in part, why dieting is largely ineffective (38, 94). Moreover, there is evidence that deiodinase dysregulation persists after weight loss (95) and may contribute to patients' well-documented propensity to regain weight. Thus, subjects striving to maintain weight loss may still require thyroid support. However, weight loss itself almost completely rescues the function of the thyroid gland in mice (**Figure 7 and Supplemental Figures 11 and 12**), inspiring hope for similar outcomes in humans.

Importantly, then, we have demonstrated—for the first time, to our knowledge—that BMI is correlated with thyroidal vascularization (**Figure 8**), similarly to what occurs in our mouse model of diet-induced obesity. *Adm*, which is closely related to *Adm2*, may be a driving factor in humans, further suggesting that our findings may well be translatable (**Supplemental Figure 13**). A limitation of this study is that the sample size was small (n = 20) and consisted almost exclusively of obese subjects (BMI = 30–40). Thus, it is possible that *Adm2* will be associated with BMI when subjects of normal weight are included. In fact, *Adm2* was recently reported to be associated with BMI and tumor aggression in patients with thyroid cancer (96). More work is needed to understand these associations and to determine whether other biochemical features of overnutrition-induced thyroid impairment in mice also occur in humans.

Thus, the work presented here has begun to fill important gaps in our knowledge using a frequently employed mouse model of diet-induced obesity. This model recapitulates the thyroid phenotype present in obese patients: increased thyroid volume, TSH levels, and serum T_3:T_4 ratio, symptoms routinely interpreted as indicating thyroid dysfunction in other contexts (19, 23, 24, 26, 27). Our findings are in line with previous research demonstrating that thyroid dysfunction can be induced by overnutrition, and adds important elements such as quantitative EM analysis, direct measurement of thyroidal THs, and metabolic analysis of TH action. Some of these changes appear to be driven by elevated TSH levels, or possibly by ectopic lipid deposition, or by both; these are phenomena that occur in a subset of obese subjects (23, 63, 64). Taken together, our findings support the emerging hypothesis that some patients may have hypothyroidism secondary to obesity, and call for deeper investigation of obesity-induced thyroid dysfunction in humans. Moreover, a recent bidirectional Mendelian randomization analysis revealed that genetically predicted high BMI was significantly associated with increased TSH levels, but not conversely (97). This issue is highly important, given the metabolic dysfunctions associated with

hypothyroidism, including reduced EE (6–10), which can exacerbate obesity. Crucially, hypothyroidism occurs early during overnutrition in our model, with signs of thyroidal stress apparent after only 10 days of overnutrition and worsening over time. This outcome has important ramifications for the many other studies using mouse models of diet-induced obesity that often last 20 weeks or longer, in which, surprisingly, THs are rarely considered. Our work furnishes a strong argument for including TH analysis in these studies, particularly for tissues that rely on serum T_4 to generate intracellular T_3. Fortunately, thyroid dysfunction in mice can be reversed by weight loss, offering hope that the same strategy could be used to repair obesity-induced thyroid damage in patients, thereby improving their metabolic regulation. Our study establishes the basic thyroidal pathophysiology needed to guide pharmacological interventions for improving thyroid function in obese patients, which will need to involve clever approaches to improving or bypassing deiodinase function.

Materials and Methods:

Sex as a biological variable

Preliminary mouse studies were performed in both sexes. The overall phenotype (systemic hypothyroidism, goiter, thyroid histology and vascularization) was similar between sexes, so remaining studies were performed with only male mice. Studies with human subjects incorporated both sexes, and BMI categories were sex-matched. Data were analyzed together because male subjects were few, due to the much higher prevalence of thyroid disease among females (2).

Animals

C57Bl/6J male and female mice were purchased from Jackson Laboratories and the colony was maintained via in-house breeding. Mice were co-housed unless otherwise noted. When 6-7 weeks old, mice were started on the study control diet (CD; Inotiv #TD.190244) to acclimate. At 8 weeks of age, about half the mice were placed on high-fat diet (HFD; 60% kcal from lard; Inotiv #TD.190243) and 5% sucrose water (collectively, the HF+SD). The sucrose water was prepared fresh every 1-2 weeks, sterile filtered, and kept at 4°C. The HFD and CD are micronutrient-matched. For the 12-week reversibility studies, the mice on the HF+SD were switched back to CD after 6 weeks. BW and each cage's food and water consumption were measured weekly, when food and water (given *ad libitum*) was refreshed. All mice were housed at 23°C on a 12-h light cycle.

Human subjects

Surgically-resected formalin-fixed paraffin-embedded (FFPE) thyroid tissues were obtained from de-identified patients treated for multinodular goiter (MNG) at Vanderbilt University Medical Center (VUMC). Bulk RNA-sequencing data from a subset of these patients was graciously provided by Dr. Vivian Weiss (VUMC).

Tissue collection

At the end of each study, mice were euthanized by exsanguination with removal of a vital organ under deep isoflurane anesthesia, and blood was collected via syringe. Organs and tissues were collected, fat depots and thyroids were weighed, and all tissues were snap frozen. Mice from each experimental group were rotated to randomize the time of tissue collection. Tissues were stored at -80°C until analysis.

Blood collection & serum preparation

Survival bleeds were performed by the retro-orbital (RO) method under deep isoflurane anesthesia using heparin-coated capillary tubes. No more than 200 µl of blood was collected over a two-week period. RO blood collection was performed between 9AM and noon to minimize possible circadian effects. End-point bleeds were performed as described in the previous section or by RO. In both cases, the blood was allowed to sit at room temperature (RT) for at least 30 min before being spun down (5000 rpm, 10 min, 4°C). Plasma and sera were then transferred to a fresh microcentrifuge tube and stored at -80°C until analysis.

TH & TSH quantitation

Plasma and sera were diluted 1:10 in 1X PBS. T_4 and T_3 were measured with commercial kits (Diagnostic Automation/Cortez Diagnostics, Inc. #9003-16 & #9001-16, respectively). Serum TSH was measured neat using a commercially available kit (Millipore #MPTMAG-49K). All were done according to the manufacturer's instructions.

Urinary I^- analysis

Mice were singly housed in urine collection cages for 48 h with *ad libitum* access to food and water. A layer of mineral oil in the collection tubes was used to block evaporation. Every 24 h, the urine was aspirated from under the mineral oil and spun down to remove particulates (3000 x g, 10 min, 4°C). The supernatants were stored at -20°C until analysis. I^- concentration was measured by colorimetric assay (BioVision #K2037-100) according to the manufacturer's instructions.

Deiodinase activity assays

The deiodinase activity assays were performed in compliance with the American Thyroid Association (ATA) guidelines (98). Tissues were homogenized in PE sucrose buffer (1 mM EDTA and 0.25 M sucrose in 1X PBS without Ca^{2+}/Mg^{2+}) on ice. Sample protein concentrations were determined by the BCA method, and then DTT was added to each sample (to a final concentration of 20 mM). The D1 activity in liver homogenates (250 µg) was assayed at 37°C with T_4 reaction solution (0.5 nM cold T_4 substrate, 20 mM DTT, and 115,000 cpm $[^{125}I]T_4$ tracer in PE sucrose buffer). BAT homogenate D2 activity was assayed under the same conditions but adding 1 mM PTU (to block any D1) and 10 nM cold T_3 (to saturate any D3). After 0.5-4 h, the reactions were stopped with horse serum. Protein and iodothyronines were precipitated with 50% TCA and spun down. Free $^{125}I^-$ in the supernatants was then measured with a gamma counter. D1 and D2 activities were calculated as I^- produced/protein content/time. D3 activity in hippocampus and cortex homogenates (25 µg) was assayed at 37°C with T_3 reaction solution (1 nM cold T_3 substrate, 20 mM DTT, and 160,000 cpm $[^{125}I]T_3$ tracer in PE sucrose buffer). The reactions were stopped with methanol and spun down to pellet the proteins. The supernatants were then filtered and passed through an ultra HPLC with an in-tandem flow scintillator detector to separate and count the $[^{125}I]T_2$ product and the $[^{125}I]T_3$ substrate. D3 activity was calculated as the amount of $[^{125}I]T_2$ produced/protein content/time. Prior to each assay, the outer ring-labeled $[^{125}I]$TH substrates were purified by Sephadex column.

Metabolic cage analysis

Male mice were kept on either the HF+SD or the CD for 4 weeks and then placed in individual metabolic cages (Sable Promethion Core) for 1 week (**Figure 2D**). Mice were acclimatized to single housing for one week prior to entering the metabolic cages and continued on their

respective diets *ad libitum* throughout. The first 48 h of metabolic cage data (acclimatization) were discarded. Data were subsequently collected for 48 h to determine each mouse's baseline EE. Mice were then implanted with an osmotic minipump (Alzet Model #2001) containing either T_3, T_4, or vehicle. T_3 and T_4 stock solutions (1.4 mM and 8 mM, respectively) were prepared in 40 mM NaOH per ATA guidelines (98) and sterile filtered. Stock solutions were diluted in sterile 0.9% saline such that final delivery rate was 1.5 µg T_4/g BW or 0.11 µg T_3/g BW per day. Control mice received vehicle-loaded minipumps. Minipumps were loaded according to the manufacturer's instructions and implanted subcutaneously above the interscapular BAT under deep isoflurane anesthesia. Mice were administered analgesia (10 mg/kg BW ketoprofen) and then returned to the metabolic cages. After one recovery day, each mouse's EE was measured over two 24-h time periods ("Day 1" & "Day 2") and compared to its baseline to calculate percent change. Average data per mouse for the baseline, Day 1, and Day 2 periods were tabulated using CalR (99). EE was calculated using the Weir equation. Because data for each mouse was normalized to that mouse's own baseline, data normalization to BW or composition was not necessary.

Thyroidal TH measurement

Proteolytic digestion of thyroid homogenates was performed to liberate the THs from TG, and their concentration in the thyroid was measured at various study endpoints, following a slightly modified published protocol (100). Briefly, deep-isoflurane-anesthetized mice were perfused transcardially with warm (35°C) 0.9% saline for 1 min to remove blood-borne THs. Thyroids were excised quickly, flash frozen in liquid nitrogen, and stored at -80°C until analysis. Next, one lobe was power homogenized in homogenizing buffer (100 mM Tris-HCl, pH 8.6; 50 mM sodium azide; 50 mM EDTA). Samples were spun down, and 150 µl supernatant was transferred to a tube containing digestion buffer and toluene. The remaining supernatant was stored for protein quantification by the BCA method to normalize results. Digested sample T_4 and T_3 were measured by immunoassay as described in a previous section. Samples were diluted ~100-fold for T_4 and ~800-fold for T_3 in digestion buffer lacking Pronase (10 parts) and toluene (1 part) so that readings fell within the linear part of the standard curve.

Fixed tissue collection for histology

Deep-isoflurane-anesthetized mice were perfused transcardially with ice-cold 1X PBS for 5-10 min to wash out blood and then fixed with 4% paraformaldehyde in 1X PBS for 5-10 min. Fixed tissues were dissected and stored in 4% paraformaldehyde at 4°C at least overnight, transferred to 70% ethanol, and then stored at RT until paraffin embedding and sectioning.

Histological staining

Fixed mouse thyroid sections (5 µm) were stained with either H&E or α-mouse CD31 antibody (Dianova #DIA310) and hematoxylin using an automated stainer (Sakura Tissue-Tek Prisma Plus and Leica Bond-RX, respectively). Some H&E stains were performed manually according to the standard protocol. Slides were imaged with a scanning brightfield microscope (Leica). De-identified screenshots of H&E stains (2-5 fields/animal in most cases) and CD31 stains (1 field/animal) were blindly scored by two independent thyroid pathologists.

ADM2 staining of fixed mouse thyroid sections (5 µm) was performed manually. Briefly, slides were de-paraffinized and rehydrated. Then, antigen retrieval was performed in boiling citrates buffer (10 mM, pH 6.0). Slides were pre-treated with 3% hydrogen peroxide, blocked with blocking solution [4% BSA (w/v) and 0.3% Triton X-100 in 1X PBS], and then incubated at 4°C overnight

with α-ADM2 antibody (Invitrogen #PA5-72030) in blocking solution. Slides were then incubated with HRP-conjugated secondary antibodies, developed with DAB substrate solution (Vector Labs #SK-4100), and counterstained with hematoxylin. Finally, slides were dehydrated, and coverslips were mounted with resin. Slides were left to air dry overnight. Negative controls were treated the same way but without primary antibody. Slides were imaged with a brightfield microscope (Leica).

H&E-stained slides of fixed human thyroid tissues were retrieved from VUMC storage. CD31 staining of human thyroid tissue was performed as described for mouse sections but with α-human CD31 antibody (Leica #PA0250). Slides were examined through a microscope and blindly scored by two independent thyroid pathologists. Representative images were taken.

Scanning electron microscopy (SEM)

Deep-isoflurane-anesthetized mice were perfused transcardially with 35°C 1X PBS without Ca^{2+}/Mg^{2+} for 30 sec at 8 mL/min to wash out blood and then fixed with 35°C SEM fixative buffer (2% glutaraldehyde, 2% paraformaldehyde, and 2 mM $CaCl_2$ in 0.1 M sodium cacodylate) for 5 min (101). The thyroid was then dissected, cut into ~1 mm^3 pieces, and postfixed in a second SEM fixative buffer (2.5% glutaraldehyde and 2 mM $CaCl_2$ in 0.1 M sodium cacodylate) for 1 h at RT. Thyroids were transferred to 1X PBS and stored at 4°C overnight. Further processing was performed as described (102). SEM-ready thyroids were cut into 100 nm-thick sections using an ultramicrotome (Leica) and placed on 10x10 mm or 5x7 mm silicon wafers (Electron Microscopy Sciences) prior to SEM imaging. Thyroid follicles were identified by their classical anatomy of a colloid-filled lumen surrounded by multi-ciliated epithelial cells (i.e., thyrocytes). Thyroid cells were mapped using large field of view SEM (Gemini2 platform, Zeiss), guided by automated tile acquisition and stitching using the Atlas 5 software (Fibics). SEM images have an X-Y resolution of 5 nm and at least 6 follicles/animal were imaged.

SEM image analysis using machine learning

To quantify thyrocyte organelle composition and anatomic parameters, we created 2D U-nets trained to identify and segment ER and mitochondria compartments, as previously described (103). Here, individual thyrocytes were manually segmented. Only thyrocytes with a visible nucleus and apical contact with colloid were chosen. U-nets were trained using Aivia software (Leica Microsystems). ER or mitochondria U-nets were trained using up to 30 individual and representative areas of thyrocyte cytosol that contained ER and mitochondria compartments. Individual ER and mitochondria were manually annotated using the LabKit plugin (ImageJ) and loaded into the U-net. The following training parameters were used: 8 layers, 64 Init Filters, 64 Filter Growth Factor, a channel reduction factor of 8, an image block size of 256x256 pixels, and an intensity threshold and area ratio threshold of 0.05. The Adam optimizer with a learning rate of 0.0001 and a staircase exponential decay for the learning rate scheduling method was used. The ER model was trained using 10,000 epochs, and the mitochondria model was trained using 600 epochs. In both models, each epoch contained 256 steps, and the balanced binary cross entropy loss function was used. The resulting trained models were applied in batch to SEM images of single thyrocytes manually segmented using ImageJ. Trained models created 32-bit pixel "organelle probability maps" that were thresholded to only include pixels with at least 80-95% classification confidence. Processed images were used to quantify relative organelle composition in each cell. The nucleus area was manually annotated (LabKit) and subtracted from the total cell area to calculate the cytoplasm area. CellProfiler's "*MeasureAreaOccupied*" function was used to determine the relative fraction of cytosol occupied by ER or mitochondria objects.

Western blotting

Frozen thyroid tissue was homogenized in 1X PBS supplemented with protease and phosphatase inhibitors (Pierce #A32959 or Halt #87786) in lysis buffer (50 mM Tris-HCl, pH 7.5; 150 mM NaCl; 5 mM EDTA; 1% Triton X-100). Thyroids from reversibility studies were homogenized in RIPA lysis buffer (50 mM Tris-HCl, pH 8.0; 150 mM NaCl; 1% IGEPAL; 0.5% sodium deoxycholate; 0.1% SDS) supplemented with protease and phosphatase inhibitors (Pierce #A32959 or Halt #87786). Samples were spun down, and the supernatant was taken for further analysis. Samples for OxPhos complexes and NIS blots were heated at 37°C for 30 min or 10 min, respectively, not boiled as the other samples. Frozen BAT was homogenized in lysis buffer (50 mM Tris-HCl, pH 7.5; 150 mM NaCl; 0.5% IGEPAL; 1 mM $Na_4P_2O_7$; 1 mM benzamidine; 5 mM Na_3VO_4; 10 mM NaF) supplemented with protease inhibitors (Sigma Roche #04693159001). Samples were spun down, and the non-fatty phase was taken for further analysis. Proteins (5-20 µg) were separated by SDS/PAGE (Bio-Rad, Invitrogen), transferred to nitrocellulose or PVDF membrane, blocked in blocking buffer (5% BSA and 0.1% Tween-20 in 1X TBS), and probed with primary antibodies against the following: BiP (CST #3177), p-eIF2α (CST #3398), eIF2α (CST #5324), CHOP (CST #2895), TG (SC #365997), PDI (CST #3501), Ero1-Lα (CST #3264), OxPhos complexes (Invitrogen #45-8099), D2 (Abcam #77779), caveolin-1 (CST #3238), & NIS (generated and affinity purified in the Carrasco lab). Some blots were stripped with either homemade stripping buffer (0.2 M glycine, 1% SDS, 0.1% Tween 20, HCl to pH 2.3) or commercial stripping buffer (Thermo #TS46436) and reprobed. The signal was developed by Pico PLUS or Femto Maximum ECL substrate (Thermo #34580 and #34094, respectively) and imaged with a ChemiDoc imaging system (Bio-Rad) and quantified using Image Lab software (Licor). Total protein imaging was done with either Ponceau S stain or stain-free technology (Bio-Rad) prior to blocking. Because TG is 50% of the protein in the thyroid (2) and it was changed by overnutrition, proteins of interest were normalized to total protein below the TG fragment bands (below ~150 kDa).

RNA-sequencing

RNA extraction (Trizol/Qiagen RNeasy) and RNA next-generation sequencing (Illumina NovaSeq 6000) of flash-frozen mouse thyroids were performed. Raw data were processed using the DESeq2 package in R. Gene set enrichment analyses were also performed in R with MSigDB gene set collections.

Human RNA-sequencing data were analyzed by the following steps: Cutadapt (v4.8) was used to trim adapter sequences from the reads. Quality control was then performed using FastQC (v0.12.1) for both raw reads and adaptor-trimmed reads. Read alignment to the Gencode GRCm38.p6 genome was performed using STAR (v2.7.11a), using Gencode vM25 gene annotations to improve the mapping accuracy. The number of reads mapped to each gene was counted with featureCounts (v2.0.6). Gene counts were normalized by DESeq2 (v1.42.1).

Triglyceride quantitation

Frozen thyroid tissue was homogenized in 1X PBS. Triglycerides were measured using a commercially available bioluminescent assay kit (Promega #J3160) according to the manufacturer's instructions.

Lipidomics

Lipid extraction and analysis by HPLC-electrospray tandem mass spectrometry of frozen thyroid

tissue were performed similarly to previously published protocols (104). Inorganic phosphate was quantitated to normalize results.

Statistical analysis and figures

Results were analyzed with GraphPad Prism software as described individually in the figure legends. GraphPad Prism was used to test the normality of data sets to aid the selection of the appropriate parametric or non-parametric statistical test. Data are presented as mean ± SD. Schematic figures were created with Biorender.

Study approval

All mouse experiments were carried out in accordance with the Vanderbilt Institutional Animal Care and Use Committee. All studies with human subjects were approved by the Institutional Review Board (IRB). This is a retrospective cohort, and it is not possible to consent these patients with historic samples.

Data availability

All data from mouse studies are available in the Supporting Data Values file, except the mouse RNA-sequencing data, which will be deposited in the GEO database. There are restrictions to the availability of patient clinical and sequencing data. This is a retrospective cohort, and it is not possible to consent these patients with historic samples. As such, the IRB has requested that we not publicly share individual-level data from each patient. The data are securely stored within a Vanderbilt patient data system. Aggregate-level data reported in this paper will be shared by Dr. Vivian Weiss upon request. Individual-level data are available only through collaboration following approval of Dr. Vivian Weiss and the VUMC IRB.

Author Contributions:

JR and NC conceived the project. QS and MAL performed the RNA-sequencing analysis with the human genetic data, and MAL performed the corresponding Pearson correlations. FSL and ACB carried out and advised on the deiodinase activity assays. RAD developed the deep learning model, and JR performed the associated manual segmentation. HW and VLW performed the histological scoring. VLW provided and oversaw access to human data. JR performed all other experimental work, with assistance from APTM and KH. JR, APTM, and NC wrote the manuscript with input from all other authors.

Acknowledgements:

We thank the members of the Carrasco laboratory for critical reading of the manuscript and insightful discussion. We also thank the following core laboratories at Vanderbilt University or Vanderbilt University Medical Center for their excellent support on this project: the Translational Pathology Shared Resource (NCI/NIH Cancer Center Support Grant P30CA068485; Shared Instrumentation Grant S10 OD023475-01A1), the Digital Histology Shared Resource, the Cell Imaging Shared Resource, the Mouse Metabolic Phenotyping Center (NIH grants DK135073 and DK020593), the Analytical Services Core, Vanderbilt Technologies for Advanced Genomics, Creative Data Solutions, and the Molecular Cell Biology Resource. This study was supported by Vanderbilt Diabetes Research & Training Center Pilot and Feasibility grant DK020593 (NC); a Vanderbilt Institute for Clinical and Translational Research grant (JR); NIH grants VCORCDP K12CA090625, K08CA240901, and R01CA272875 (VLW); NIH grants 1F30CA281125-01 and

T32GM007347 (MAL); American Cancer Society grants RSG-22-084-01-MM and 133934-CSDG-19-216-01-TBG (VLW); and ATA grant 2019-0000000090 (VLW).

References:

1. Mullur R, Liu Y-Y, Brent GA. Thyroid Hormone Regulation of Metabolism. *Physiol Rev*. 2014;94(2):355–382.

2. Boron W, Boulpaep E. *Medical Physiology*. Philadelphia, PA: Elsevier; 2017.

3. Dai G, Levy O, Carrasco N. Cloning and characterization of the thyroid iodide transporter. *Nature*. 1996;379(6564):458–460.

4. Portulano C, Paroder-Belenitsky M, Carrasco N. The Na+/I− Symporter (NIS): Mechanism and Medical Impact. *Endocr Rev*. 2014;35(1):106–149.

5. Ravera S, et al. The Sodium/Iodide Symporter (NIS): Molecular Physiology and Preclinical and Clinical Applications. *Annu Rev Physiol*. 2017;79(1):261–289.

6. DuBois EF. *Basal Metabolism in Health and Disease*. Philadelphia: Lea & Febiger; 1927.

7. al-Adsani H, Hoffer LJ, Silva JE. Resting energy expenditure is sensitive to small dose changes in patients on chronic thyroid hormone replacement. *J Clin Endocrinol Metab*. 1997;82(4):1118–25.

8. Duntas LH. Thyroid Disease and Lipids. *Thyroid*. 2002;12(4):287–293.

9. Biondi B, Klein I. Hypothyroidism as a risk factor for cardiovascular disease. *Endocrine*. 2004;24(1):1–13.

10. Chung GE, et al. Non-alcoholic fatty liver disease across the spectrum of hypothyroidism. *J Hepatol*. 2012;57(1):150–156.

11. Ferrandino G, et al. Pathogenesis of hypothyroidism-induced NAFLD is driven by intra- and extrahepatic mechanisms. *Proceedings of the National Academy of Sciences*. 2017;114(43):E9172–E9180.

12. Biondi B, Cappola AR, Cooper DS. Subclinical Hypothyroidism: A Review. *JAMA*. 2019;322(2):153–160.

13. Fox CS, et al. Relations of thyroid function to body weight: Cross-sectional and longitudinal observations in a community-based sample. *Arch Intern Med*. 2008;168(6). https://doi.org/10.1001/archinte.168.6.587.

14. Knudsen N, et al. Small Differences in Thyroid Function May Be Important for Body Mass Index and the Occurrence of Obesity in the Population. *J Clin Endocrinol Metab*. 2005;90(7):4019–4024.

15. Carlé A, et al. Smoking cessation is followed by a sharp but transient rise in the incidence of overt autoimmune hypothyroidism – A population-based, case–control study. *Clin Endocrinol (Oxf)*. 2012;77(5):764–772.

16. Pasquali R, et al. European Society of Endocrinology Clinical Practice Guideline: Endocrine work-up in obesity. *Eur J Endocrinol*. 2020;182(1):G1–G32.

17. Karmisholt J, Andersen S, Laurberg P. Weight loss after therapy of hypothyroidism is mainly caused by excretion of excess body water associated with myxoedema. *J Clin Endocrinol Metab*.

2011;96(1). https://doi.org/10.1210/JC.2010-1521.

18. van Hulsteijn LT, et al. Prevalence of endocrine disorders in obese patients: systematic review and meta-analysis. *Eur J Endocrinol*. 2020;182(1):11–21.

19. Wesche MFT, Wiersinga WM, Smits NJ. Lean body mass as a determinant of thyroid size. *Clin Endocrinol (Oxf)*. 1998;48(6). https://doi.org/10.1046/j.1365-2265.1998.00400.x.

20. Loy M, et al. Correlation of Computerized Gray-scale Sonographic Findings with Thyroid Function and Thyroid Autoimmune Activity in Patients with Hashimoto's Thyroiditis. *Journal of Clinical Ultrasound*. 2004;32(3). https://doi.org/10.1002/jcu.20008.

21. Rotondi M, et al. A hypoechoic pattern of the thyroid at ultrasound does not indicate autoimmune thyroid diseases in patients with morbid obesity. *Eur J Endocrinol*. 2010;163(1). https://doi.org/10.1530/EJE-10-0288.

22. Radetti G, et al. Thyroid function and structure are affected in childhood obesity. *Journal of Clinical Endocrinology and Metabolism*. 2008;93(12). https://doi.org/10.1210/jc.2008-0823.

23. Guan B, et al. Effect of Bariatric Surgery on Thyroid Function in Obese Patients: a Systematic Review and Meta-Analysis. *Obes Surg*. 2017;27(12):3292–3305.

24. Sari R, et al. The effect of body weight and weight loss on thyroid volume and function in obese women. *Clin Endocrinol (Oxf)*. 2003;59(2):258–262.

25. Kyrou I, et al. Improved thyroid hypoechogenicity following bariatric-induced weight loss in euthyroid adults with severe Obesity-a pilot study. *Front Endocrinol (Lausanne)*. 2018;9(AUG). https://doi.org/10.3389/fendo.2018.00488.

26. Garber JR, et al. Clinical practice guidelines for hypothyroidism in adults: Cosponsored by the American Association of clinical endocrinologists and the American Thyroid Association. *Thyroid*. 2012;22(12):1200–1235.

27. Eastman CJ, Zimmermann MB. The Iodine Deficiency Disorders. *Endotext*. [published online ahead of print: April 24, 2015]. http://europepmc.org/books/NBK285556. Accessed November 10, 2024.

28. Vagenakis G, et al. Studies of serum triiodothyronine, thyroxine and thyrotropin concentrations in endemic goiter in greece. *Journal of Clinical Endocrinology and Metabolism*. 1973;37(3). https://doi.org/10.1210/jcem-37-3-485.

29. Danforth E, et al. Dietary-induced alterations in thyroid hormone metabolism during overnutrition. *J Clin Invest*. 1979;64(5):1336–47.

30. Utiger RD. Differing thyrotropin responses to increased serum triiodothyronine concentrations produced by overfeeding and by triiodothyronine administration. *Metabolism*. 1982;31(2). https://doi.org/10.1016/0026-0495(82)90132-9.

31. Poehlman ET, et al. Genotype dependency of the thermic effect of a meal and associated hormonal changes following short-term overfeeding. *Metabolism*. 1986;35(1). https://doi.org/10.1016/0026-0495(86)90092-2.

32. Danforth E, Burger AG. The impact of nutrition on thyroid hormone physiology and action.

Annu Rev Nutr. 1989;9(1). https://doi.org/10.1146/annurev.nu.09.070189.001221.

33. Bianco AC, et al. Paradigms of Dynamic Control of Thyroid Hormone Signaling. *Endocr Rev*. 2019;40(4):1000.

34. Maia AL, et al. Type 2 iodothyronine deiodinase is the major source of plasma T3 in euthyroid humans. *J Clin Invest*. 2005;115(9):2524–33.

35. Bray GA, Bouchard C. The biology of human overfeeding: A systematic review. *Obesity Reviews*. 2020;21(9). https://doi.org/10.1111/obr.13040.

36. Bandini LG, et al. Energy expenditure during carbohydrate overfeeding in obese and nonobese adolescents. *Am J Physiol Endocrinol Metab*. 1989;256(3). https://doi.org/10.1152/ajpendo.1989.256.3.e357.

37. Katzeff HL, et al. Metabolic studies in human obesity during overnutrition and undernutrition: Thermogenic and hormonal responses to norepinephrine. *Metabolism*. 1986;35(2). https://doi.org/10.1016/0026-0495(86)90119-8.

38. Rosenbaum M, et al. Low-dose leptin reverses skeletal muscle, autonomic, and neuroendocrine adaptations to maintenance of reduced weight. *Journal of Clinical Investigation*. 2005;115(12):3579–3586.

39. Visser TJ. Role of sulfation in thyroid hormone metabolism. *Chem Biol Interact*. 1994;92(1–3):293–303.

40. Peeters RP, Visser TJ. Metabolism of Thyroid Hormone. *New Comprehensive Biochemistry*. 2017;18:81–103.

41. Citterio CE, Targovnik HM, Arvan P. The role of thyroglobulin in thyroid hormonogenesis. *Nature Reviews Endocrinology 2019 15:6*. 2019;15(6):323–338.

42. Marine D, Lenhart CH. The pathological anatomy of the human thyroid gland. *The Archives of Internal Medicine*. 1911;7(4):506–535.

43. Rowlands AG, Panniers R, Henshaw EC. The catalytic mechanism of guanine nucleotide exchange factor action and competitive inhibition by phosphorylated eukaryotic initiation factor 2. *Journal of Biological Chemistry*. 1988;263(12). https://doi.org/10.1016/s0021-9258(18)60596-4.

44. Hetz C. The unfolded protein response: controlling cell fate decisions under ER stress and beyond. *Nature Reviews Molecular Cell Biology 2012 13:2*. 2012;13(2):89–102.

45. Ozcan U, et al. Endoplasmic Reticulum Stress Links Obesity, Insulin Action, and Type 2 Diabetes. *Science (1979)*. 2004;306(5695):457–461.

46. Kharroubi I, et al. Free fatty acids and cytokines induce pancreatic beta-cell apoptosis by different mechanisms: role of nuclear factor-kappaB and endoplasmic reticulum stress. *Endocrinology*. 2004;145(11):5087–5096.

47. Hammerschmidt P, Brüning JC. Contribution of specific ceramides to obesity-associated metabolic diseases. *Cell Mol Life Sci*. 2022;79(8). https://doi.org/10.1007/S00018-022-04401-3.

48. Tam AB, et al. The UPR Activator ATF6 Responds to Proteotoxic and Lipotoxic Stress by Distinct Mechanisms. *Dev Cell*. 2018;46(3):327-343.e7.

49. Smith RS, et al. Intermedin is a new angiogenic growth factor. *Am J Physiol Heart Circ Physiol*. 2009;297(3). https://doi.org/10.1152/AJPHEART.00404.2009/ASSET/IMAGES/LARGE/ZH40090990020007.JPEG.

50. Takei Y, et al. Identification of novel adrenomedullin in mammals: A potent cardiovascular and renal regulator. *FEBS Lett*. 2004;556(1–3). https://doi.org/10.1016/S0014-5793(03)01368-1.

51. Fischer J-P, Els-Heindl S, Beck-Sickinger AG. Adrenomedullin – Current perspective on a peptide hormone with significant therapeutic potential. *Peptides (NY)*. 2020;131:170347.

52. Nagasaki S, et al. Induction of adrenomedullin 2/intermedin expression by thyroid stimulating hormone in thyroid. *Mol Cell Endocrinol*. 2014;395(1–2):32–40.

53. Thomas Bigos S, et al. Spectrum of pituitary alterations with mild and severe thyroid impairment. *Journal of Clinical Endocrinology and Metabolism*. 1978;46(2). https://doi.org/10.1210/jcem-46-2-317.

54. Meda C, et al. Hepatic ERα accounts for sex differences in the ability to cope with an excess of dietary lipids. *Mol Metab*. 2020;32:97.

55. Citterio CE, et al. De novo triiodothyronine formation from thyrocytes activated by thyroid-stimulating hormone. *Journal of Biological Chemistry*. 2017;292(37):15434–15444.

56. Lavado-Autric R, et al. Deiodinase activities in thyroids and tissues of iodine-deficient female rats. *Endocrinology*. 2013;154(1). https://doi.org/10.1210/en.2012-1727.

57. Toyoda N, et al. Graves' immunoglobulin G stimulates iodothyronine 5′-deiodinating activity in FRTL-5 rat thyroid cells. *Journal of Clinical Endocrinology and Metabolism*. 1990;70(6). https://doi.org/10.1210/jcem-70-6-1506.

58. Shrestha S, et al. Aging compromises human islet beta cell function and identity by decreasing transcription factor activity and inducing ER stress. *Sci Adv*. 2022;8(40). https://doi.org/10.1126/SCIADV.ABO3932/SUPPL_FILE/SCIADV.ABO3932_TABLES_S1_TO_S8.ZIP.

59. Citterio CE, Rivolta CM, Targovnik HM. Structure and genetic variants of thyroglobulin: Pathophysiological implications. *Mol Cell Endocrinol*. 2021;528:111227.

60. El-Sayed SM, Ibrahim HM. Effect of high-fat diet-induced obesity on thyroid gland structure in female rats and the possible ameliorating effect of metformin therapy. *Folia Morphol (Warsz)*. 2020;79(3):476–488.

61. Shao SS, et al. Dietary high-fat lard intake induces thyroid dysfunction and abnormal morphology in rats. *Acta Pharmacol Sin*. 2014;35(11):1411–1420.

62. Zhang X, et al. ER stress contributes to high-fat diet-induced decrease of thyroglobulin and hypothyroidism. *Am J Physiol Endocrinol Metab*. 2019;316(3):E510–E518.

63. Lee MH, et al. Thyroid dysfunction associated with follicular cell steatosis in obese male mice and humans. *Endocrinology*. 2015;156(3):1181–1193.

64. Basolo A, et al. Histological pattern and gene expression profiling of thyroid tissue in subjects

with obesity. *J Endocrinol Invest*. 2022;45(2). https://doi.org/10.1007/s40618-021-01662-w.

65. Di Jeso B, Arvan P. Thyroglobulin from molecular and cellular biology to clinical endocrinology. *Endocr Rev*. 2016;37(1). https://doi.org/10.1210/er.2015-1090.

66. Castillo M, et al. Disruption of Thyroid Hormone Activation in Type 2 Deiodinase Knockout Mice Causes Obesity With Glucose Intolerance and Liver Steatosis Only at Thermoneutrality. *Diabetes*. 2011;60(4):1082–1089.

67. Marsili A, et al. Mice with a Targeted Deletion of the Type 2 Deiodinase Are Insulin Resistant and Susceptible to Diet Induced Obesity. *PLoS One*. 2011;6(6):e20832.

68. de Jesus LA, et al. The type 2 iodothyronine deiodinase is essential for adaptive thermogenesis in brown adipose tissue. *Journal of Clinical Investigation*. 2001;108(9):1379–1385.

69. Mentuccia D, et al. Association between a novel variant of the human type 2 deiodinase gene Thr92Ala and insulin resistance: evidence of interaction with the Trp64Arg variant of the beta-3-adrenergic receptor. *Diabetes*. 2002;51(3):880–3.

70. Canani LH, et al. The Type 2 Deiodinase A/G (Thr92Ala) Polymorphism Is Associated with Decreased Enzyme Velocity and Increased Insulin Resistance in Patients with Type 2 Diabetes Mellitus. *J Clin Endocrinol Metab*. 2005;90(6):3472–3478.

71. Salvatore D, et al. Molecular biological and biochemical characterization of the human type 2 selenodeiodinase. *Endocrinology*. 1996;137(8):3308–3315.

72. Salvatore D, et al. Thyroid hormones and skeletal muscle—new insights and potential implications. *Nat Rev Endocrinol*. 2014;10(4):206–214.

73. Müller TD, et al. Anti-Obesity Therapy: from Rainbow Pills to Polyagonists. *Pharmacol Rev*. 2018;70(4):712–746.

74. Yoneshiro T, et al. Recruited brown adipose tissue as an antiobesity agent in humans. *J Clin Invest*. 2013;123(8):3404–8.

75. Hanssen MJW, et al. Short-term Cold Acclimation Recruits Brown Adipose Tissue in Obese Humans. *Diabetes*. 2016;65(5):1179–1189.

76. Watanabe M, et al. Bile acids induce energy expenditure by promoting intracellular thyroid hormone activation. *Nature*. 2006;439(7075):484–489.

77. Broeders EPM, et al. The bile acid chenodeoxycholic acid increases human brown adipose tissue activity. *Cell Metab*. 2015;22(3):418–426.

78. Vijgen GHEJ, et al. Brown adipose tissue in morbidly obese subjects. *PLoS One*. 2011;6(2). https://doi.org/10.1371/journal.pone.0017247.

79. Saito M, et al. High incidence of metabolically active brown adipose tissue in healthy adult humans: Effects of cold exposure and adiposity. *Diabetes*. 2009;58(7). https://doi.org/10.2337/db09-0530.

80. Vijgen GHEJ, et al. Increase in brown adipose tissue activity after weight loss in morbidly obese subjects. *Journal of Clinical Endocrinology and Metabolism*. 2012;97(7). https://doi.org/10.1210/jc.2012-1289.

81. Jastreboff AM, et al. Tirzepatide Once Weekly for the Treatment of Obesity. *New England Journal of Medicine*. 2022;387(3). https://doi.org/10.1056/nejmoa2206038.

82. Lum SMC, et al. Peripheral tissue mechanism for maintenance of serum triiodothyronine values in a thyroxine-deficient state in man. *Journal of Clinical Investigation*. 1984;73(2). https://doi.org/10.1172/JCI111245.

83. Salas-Lucia F, Bianco AC. T3 levels and thyroid hormone signaling. *Front Endocrinol (Lausanne)*. 2022;13. https://doi.org/10.3389/fendo.2022.1044691.

84. Penna GC, et al. Thyroid Hormone Homeostasis in Levothyroxine-treated Patients: Findings From ELSA-Brasil. *J Clin Endocrinol Metab*. [published online ahead of print: 2024]. https://doi.org/10.1210/clinem/dgae139.

85. Galton VA, et al. Life without Thyroxine to 3,5,3′-Triiodothyronine Conversion: Studies in Mice Devoid of the 5′-Deiodinases. *Endocrinology*. 2009;150(6):2957–2963.

86. Gereben B, et al. Cellular and Molecular Basis of Deiodinase-Regulated Thyroid Hormone Signaling. *Endocr Rev*. 2008;29(7):898–938.

87. Biondi B. Subclinical Hypothyroidism in Patients with Obesity and Metabolic Syndrome: A Narrative Review. *Nutrients*. 2024;16(1). https://doi.org/10.3390/nu16010087.

88. Finan B, et al. Chemical Hybridization of Glucagon and Thyroid Hormone Optimizes Therapeutic Impact for Metabolic Disease. *Cell*. 2016;167(3):843-857.e14.

89. Harrison SA, et al. A Phase 3, Randomized, Controlled Trial of Resmetirom in NASH with Liver Fibrosis. *New England Journal of Medicine*. 2024;390(6):497–509.

90. Chen K, et al. Adipose-targeted triiodothyronine therapy counteracts obesity-related metabolic complications and atherosclerosis with negligible side effects. *Nat Commun*. 2022;13(1). https://doi.org/10.1038/s41467-022-35470-4.

91. Reinehr T, et al. Thyroid hormones and their relation to weight status. *Horm Res*. 2008;70(1):51–7.

92. Vagenakis A, Braverman L, Merimee TJ. Acute effects of starvation on thyroid hormone concentrations in peripheral blood. *Clin Res*. 1975;23(3).

93. Vagenakis AG, et al. Effect of Starvation on the Production and Metabolism of Thyroxine and Triiodothyronine in Euthyroid Obese Patients. *J Clin Endocrinol Metab*. 1977;45(6):1305–1309.

94. Rosenbaum M, et al. Effects of changes in body weight on carbohydrate metabolism, catecholamine excretion, and thyroid function. *Am J Clin Nutr*. 2000;71(6):1421–1432.

95. Di Munno C, et al. Adaptive Thermogenesis Driving Catch-Up Fat Is Associated With Increased Muscle Type 3 and Decreased Hepatic Type 1 Iodothyronine Deiodinase Activities: A Functional and Proteomic Study. *Front Endocrinol (Lausanne)*. 2021;0:27.

96. Kim JT, et al. Adrenomedullin2 stimulates progression of thyroid cancer in mice and humans under nutrient excess conditions. *J Pathol*. 2022;258(3):264–277.

97. Wang X, et al. Causal association between serum thyrotropin and obesity: A bidirectional, mendelian randomization study. *Journal of Clinical Endocrinology and Metabolism*. 2021;106(10).

https://doi.org/10.1210/clinem/dgab183.

98. Bianco AC, et al. American Thyroid Association Guide to Investigating Thyroid Hormone Economy and Action in Rodent and Cell Models. *Thyroid*. 2014;24(1):88–168.

99. Mina AI, et al. CalR: A Web-Based Analysis Tool for Indirect Calorimetry Experiments. *Cell Metab*. 2018;28(4):656-666.e1.

100. Liu C, et al. Hypothyroidism induced by loss of the manganese efflux transporter SLC30A10 may be explained by reduced thyroxine production. *Journal of Biological Chemistry*. 2017;292(40):16605–16615.

101. Arrojo e Drigo R, et al. Age Mosaicism across Multiple Scales in Adult Tissues. *Cell Metab*. 2019;30(2):343-351.e3.

102. Dos Santos C, et al. Calorie restriction increases insulin sensitivity to promote beta cell homeostasis and longevity in mice. *Nature Communications 2024 15:1*. 2024;15(1):1–22.

103. Winn NC, et al. Weight Cycling Impairs Pancreatic Insulin Secretion but Does Not Perturb Whole-Body Insulin Action in Mice With Diet-Induced Obesity. *Diabetes*. 2022;71(11):2313–2330.

104. Ren J, et al. Orm proteins control ceramide synthesis and endocytosis via LCB-mediated Ypk1 regulation. *J Lipid Res*. 2024;100683.

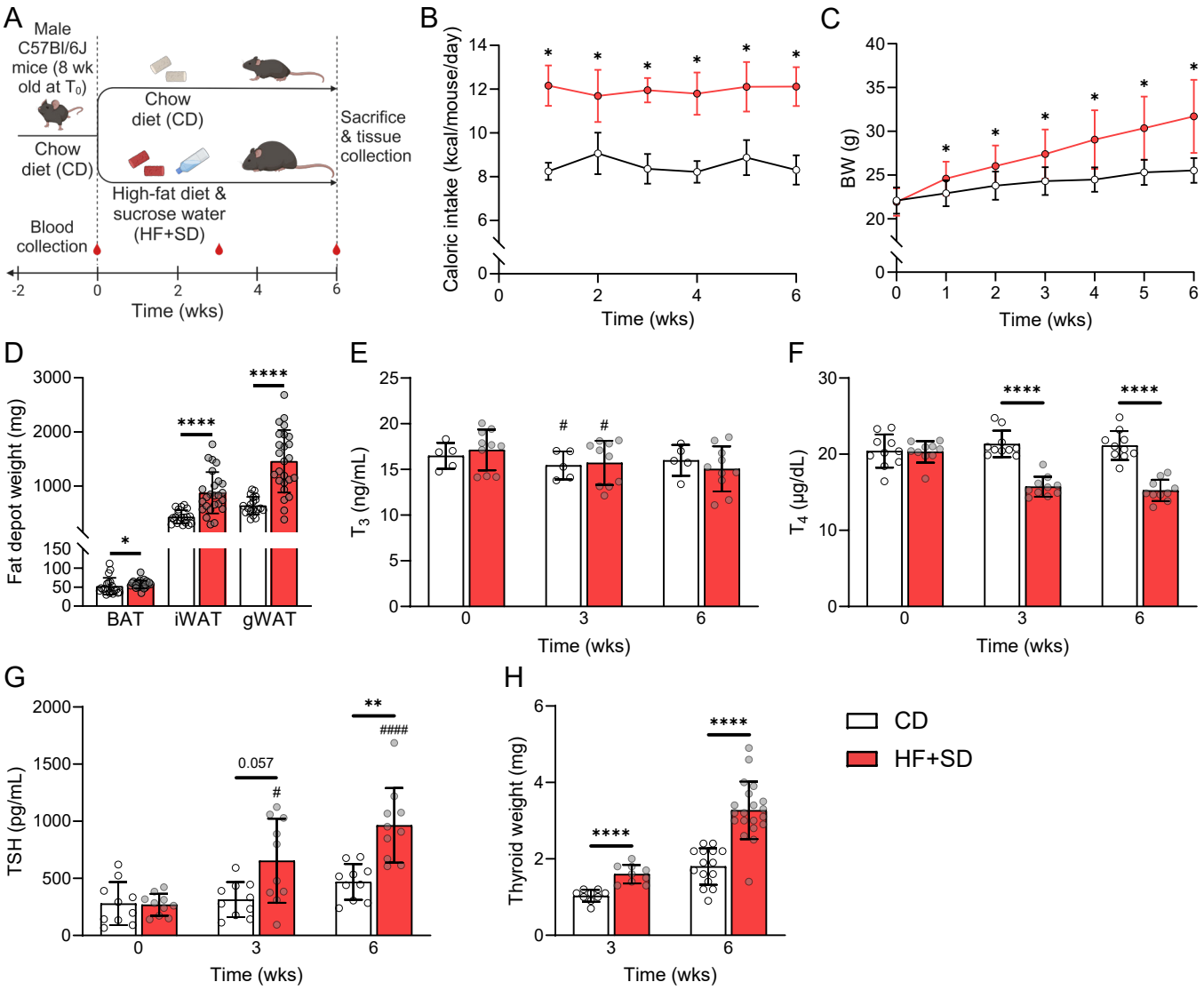

Figure 1. Overnutrition induces hypothyroidism and goiter. All studies followed this general design (A) unless otherwise specified. Caloric intake (B) and BW (C) were measured weekly. BAT, inguinal white adipose tissue (iWAT), and gonadal WAT (gWAT) depots were weighed immediately after dissection (D). Plasma and sera were analyzed by immunoassay for total T_3 (E), total T_4 (F) and TSH (G). Thyroids were carefully dissected at either week 3 or week 6 and weighed (H). All data are representative of at least two separate cohorts of mice. CD n = 20, HF+SD n = 25 (B–D). Data were analyzed by 2-way ANOVA with multiple comparisons (B, C, E–G), unpaired Student's t-test with Welch's correction (D: WAT, H), or Mann-Whitney test (D: BAT). *$p < 0.05$, **$p < 0.01$, & ****$p < 0.0001$ vs. controls within that timepoint. #$p < 0.05$ & ####$p < 0.0001$ vs. week 0 within that diet group.

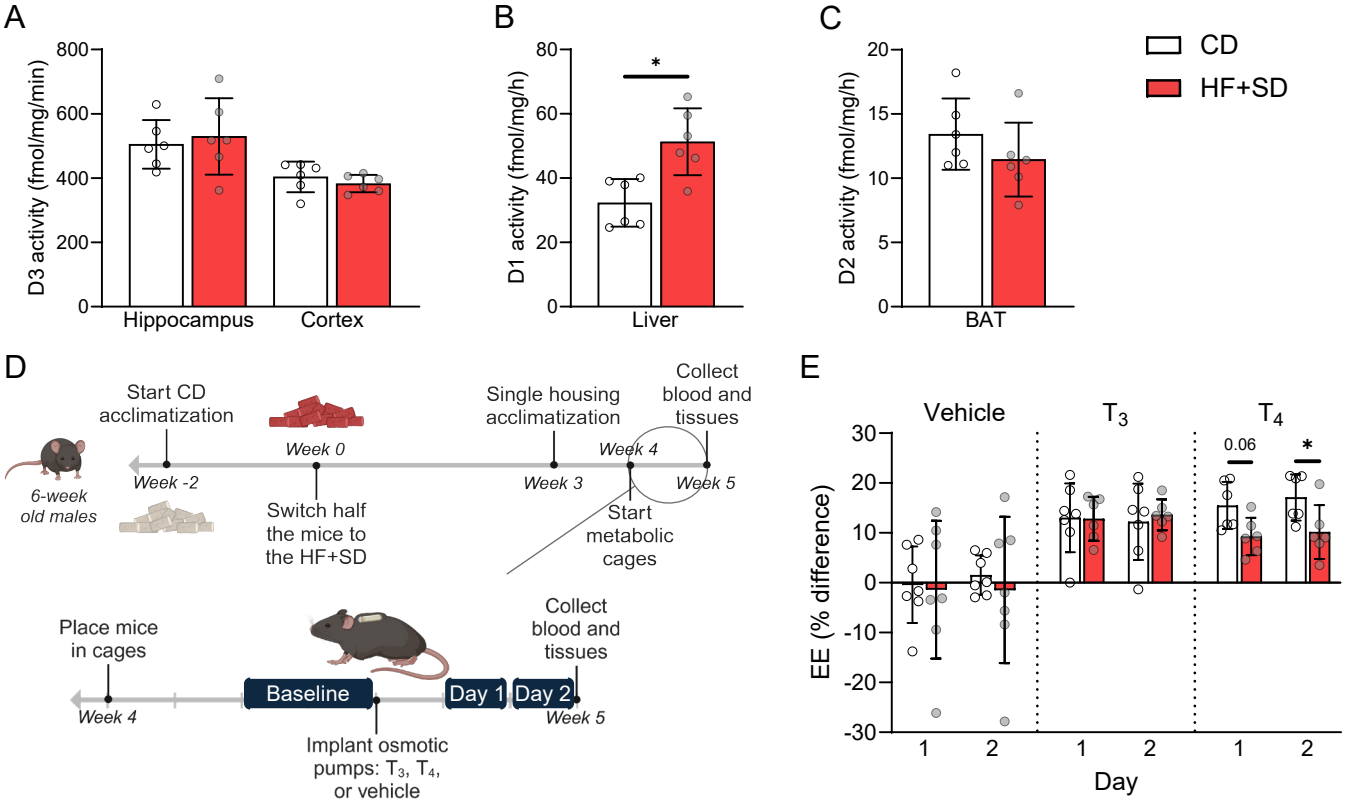

Figure 2. Overnutrition modulates deiodinase activity, overall reducing whole-body T_4-to-T_3 conversion and EE. Deiodination rates mediated by D3 in hippocampus and cortex (A), D1 in liver (B), and D2 in BAT (C) were measured. The metabolic cage study design is shown (D). EE was measured at baseline for 48 h and then in response to vehicle, T_3, or T_4 for two 24-h time periods ("Day 1" and "Day 2") after osmotic minipump implantation. The percent difference of the average EE between the response "Days" and baseline was then calculated for each mouse (E). Data were analyzed by unpaired Student's *t*-test with Welch's correction (A–C) or 2-way ANOVA with multiple comparisons (E). *$p < 0.05$ & **$p < 0.01$.

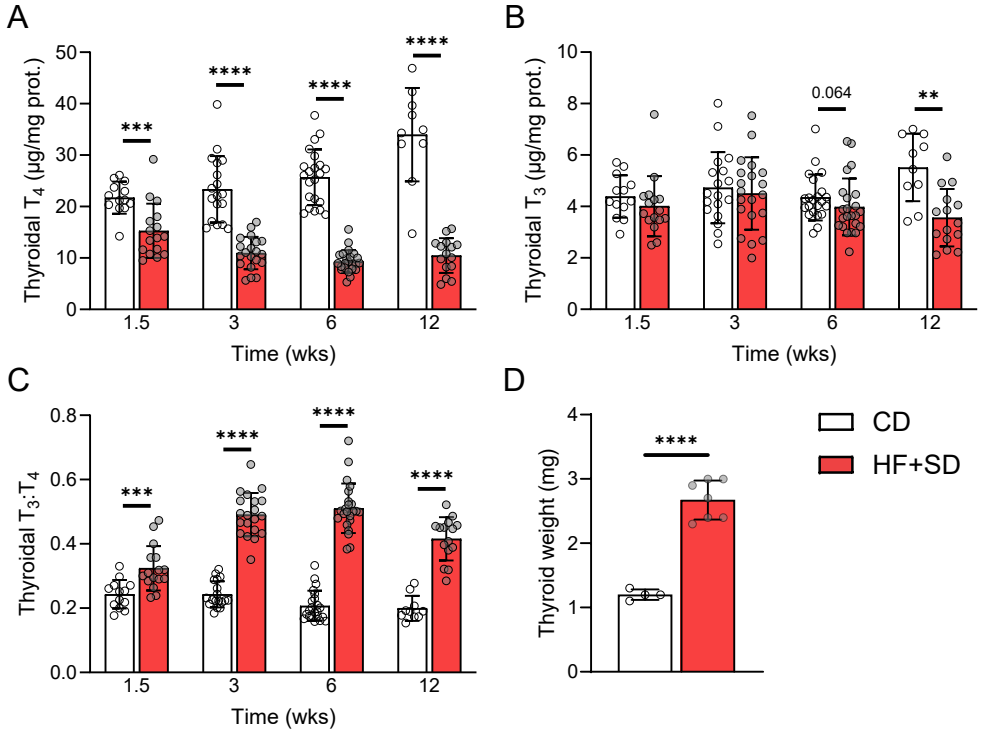

Figure 3. Overnutrition directly impairs TH biosynthesis. Male mice were placed on the HF+SD or CD for up to 12 weeks. At each timepoint, thyroids were collected and fully proteolyzed. Liberated T_4 (A) and T_3 (B) were measured by immunoassay and normalized to the thyroidal protein. The thyroidal T_3:T_4 ratio was calculated (C). At the 12-week timepoint, some thyroids were collected and weighed (D). Data represent 2-3 separate cohorts of mice per timepoint, CD n = 10-22, HF+SD n = 15-23 (A–C). Data were analyzed per timepoint by unpaired Student's t-test with Welch's correction or Mann-Whitney test, based on normality. **$p < 0.01$, ***$p < 0.001$, & ****$p < 0.0001$ vs. controls at that timepoint.

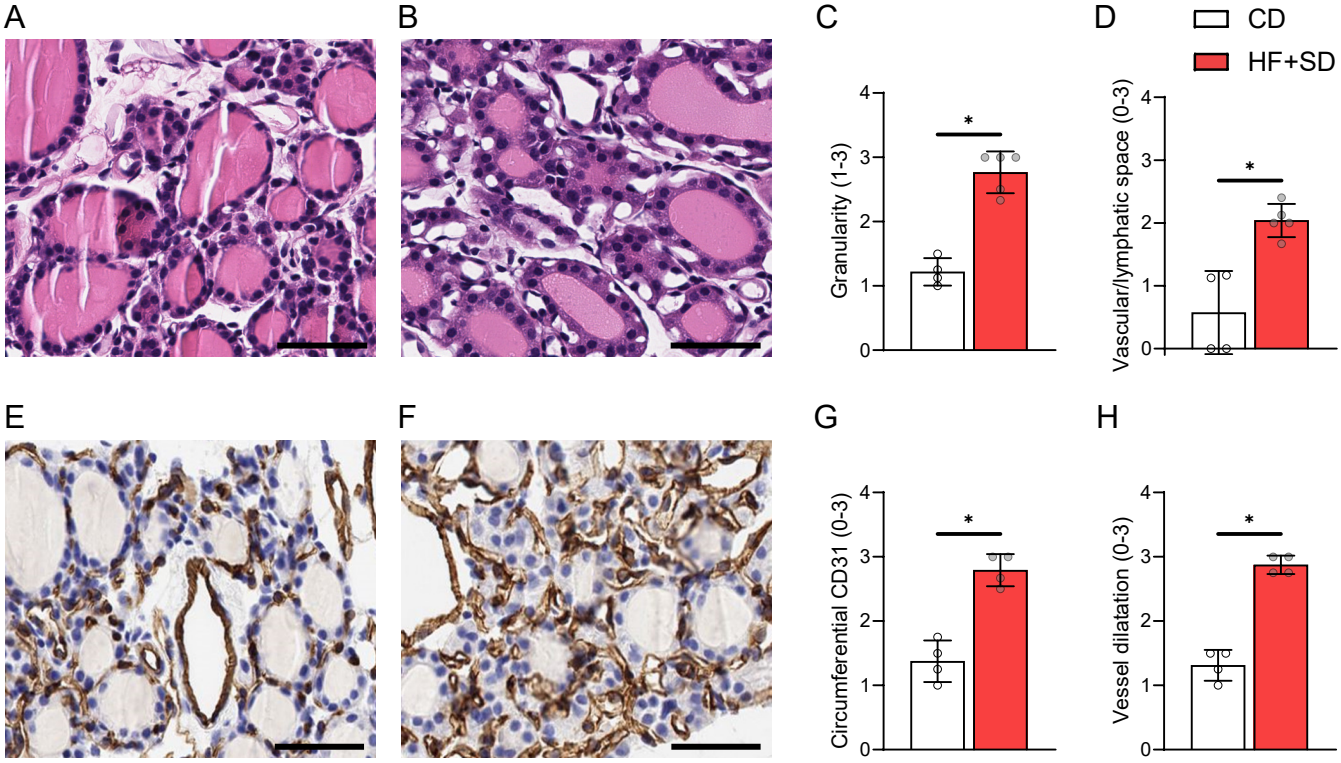

Figure 4. Overnutrition leads to hypertrophy, increased granularity, and increased vascularization of thyrocytes. Representative H&E images from the CD (A) and HF+SD (B) groups are shown. H&E images were blindly scored for extent of granularity (C) and interfollicular vascular/ lymphatic space (D). Fixed thyroid sections were also stained for CD31, a vascular marker, and images from CD mice (E) and HF+SD mice (F) were blindly scored for extent of circumferential staining around the follicles (G) and dilatation of the follicular microcapillaries (H). Scale bars = 50 μm. Data were analyzed by Mann-Whitney test. *$p < 0.05$.

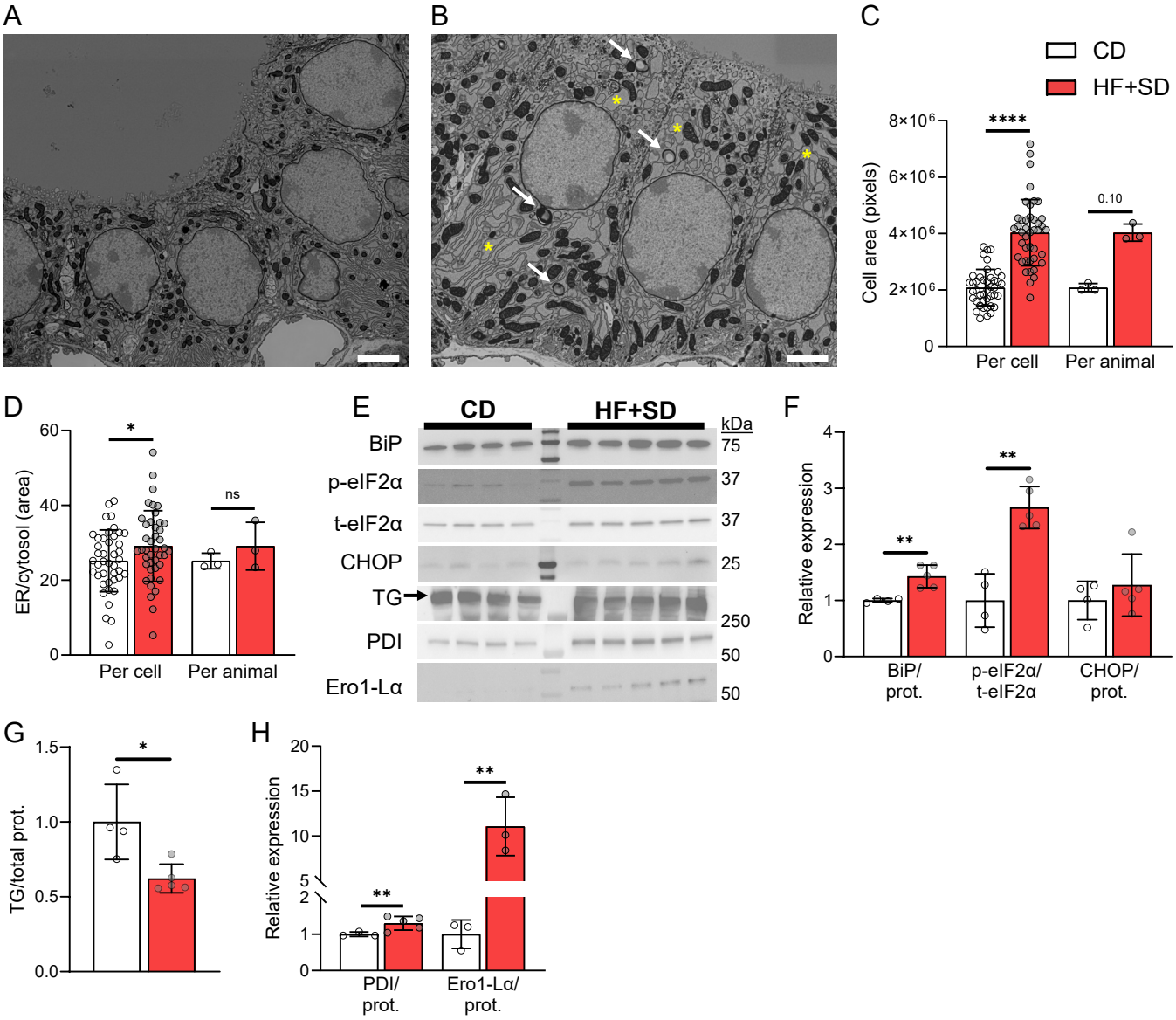

Figure 5. Overnutrition induces thyroidal ER stress and reduces TG. Thyroids were processed for electron microscopy (EM). Representative images from a CD mouse (A) and a HF+SD mouse (B) are shown. Yellow asterisks label a few examples of bloated ER. White arrows point to lipid droplets. A deep learning model was used to quantitate thyrocyte total area (C) and ER area relative to cytosol area (D). Western blots of thyroid homogenate (E) were performed and quantitated for ER stress markers (F), TG (G), and TG folding chaperones (H). Scale bars = 2.5 µm. EM data are presented per cell (n = 42/group) and as the average of the 14 cells/animal. Data were analyzed by unpaired Student's t-test with Welch's correction or Mann-Whitney test, based on normality. *$p < 0.05$, **$p < 0.01$, & ****$p < 0.0001$.

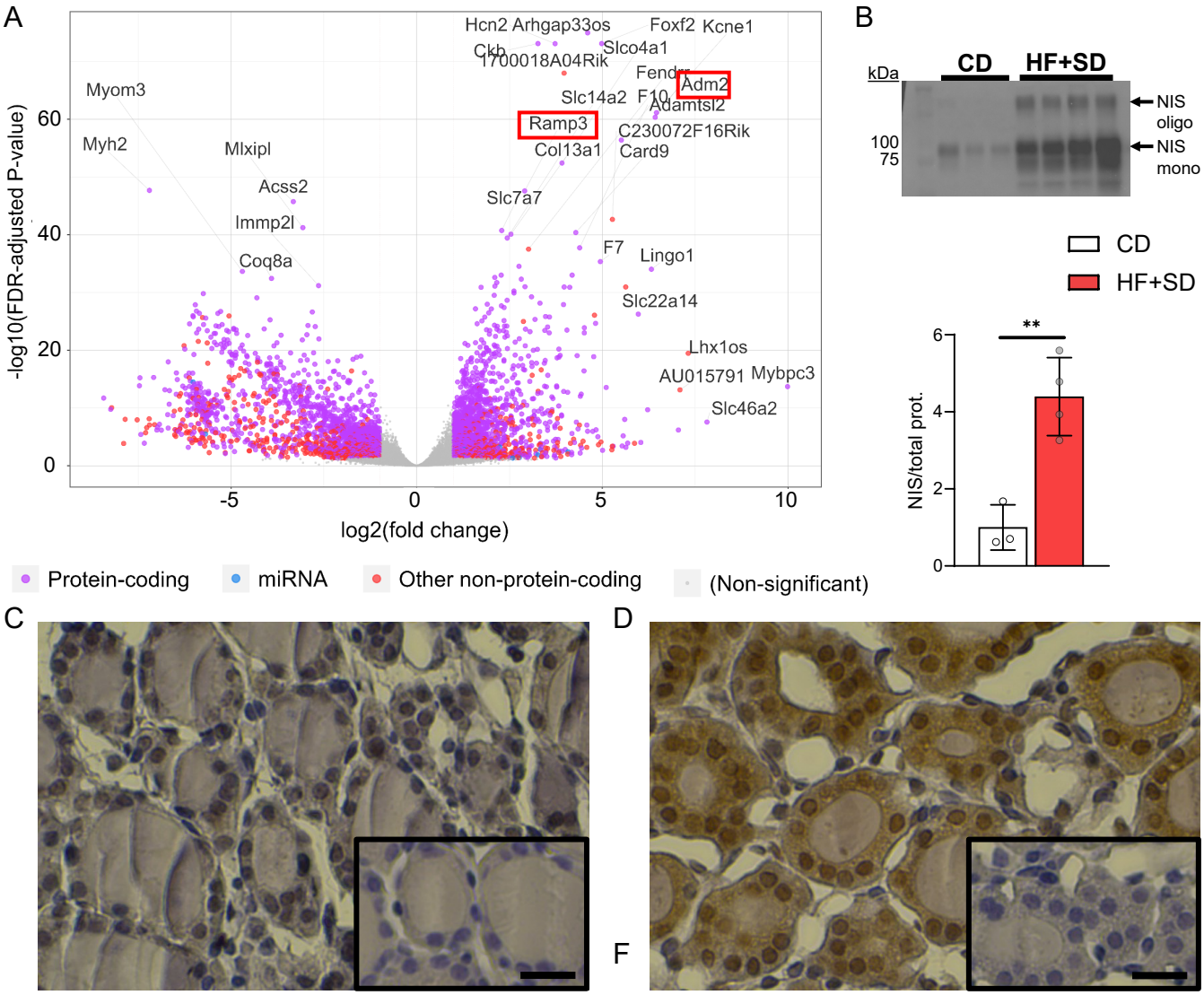

Figure 6. High TSH signaling appears unimpaired and likely drives thyroidal vascularization by upregulating thyrocyte ADM2 expression. Thyroids were processed for RNA sequencing. Differential gene expression analysis yielded over 6,000 genes (A). Western blot of thyroid homogenate was performed for NIS and quantitated (B). The arrow indicates fully glycosylated NIS. The other bands correspond to oligomeric forms and partially glycosylated NIS. Fixed thyroid sections were stained for ADM2, and representative images from the CD (C) and HF+SD (D) groups are shown (insets: negative controls lacking primary antibody). Scale bars = 20 μm. CD n = 3, HF+SD n = 4, $\log_2$ fold change > 1, & false discovery rate-adjusted p-value < 0.05 (A). Data were analyzed by unpaired Student's t-test with Welch's correction (B). $^{**}p < 0.01$.

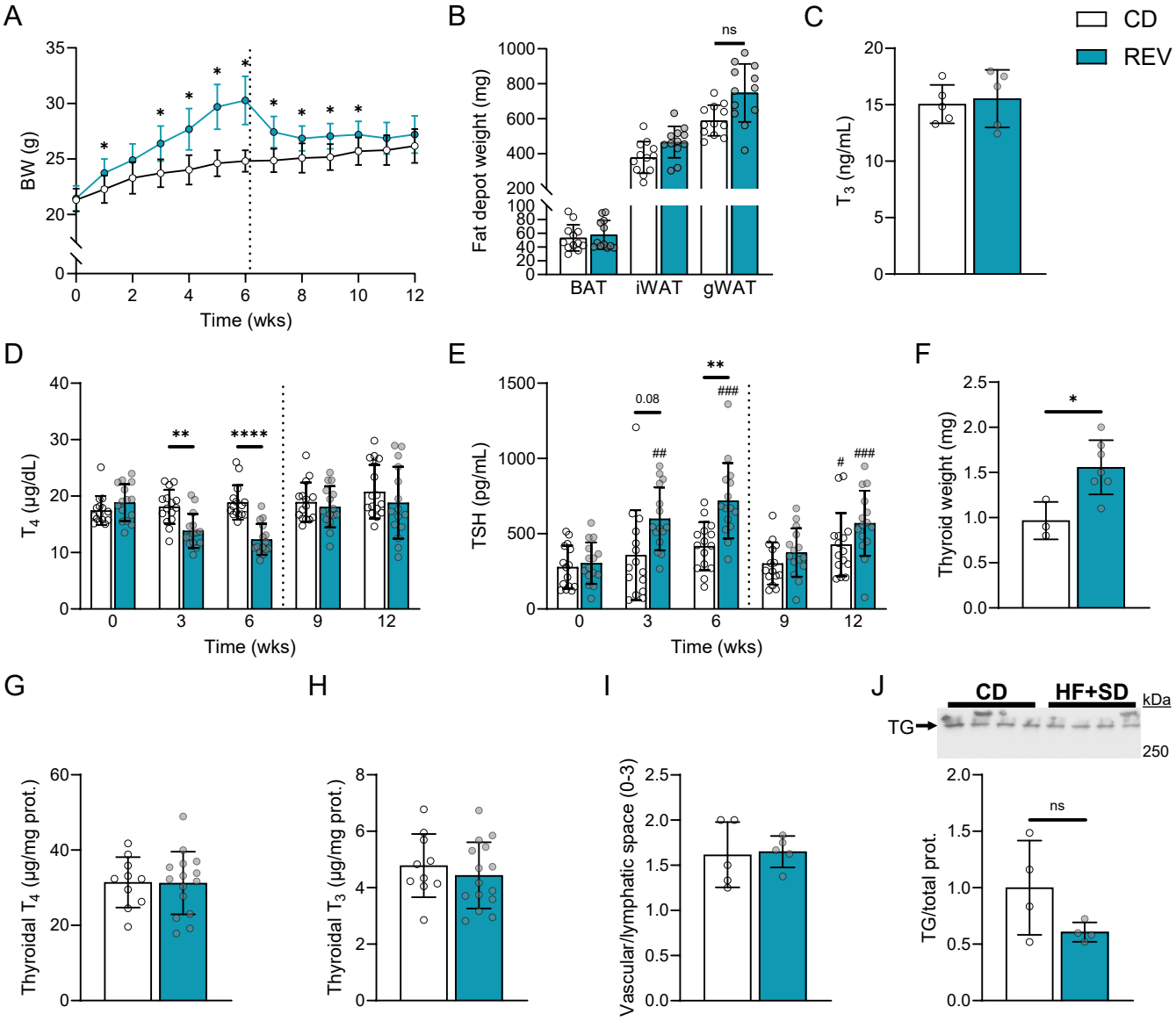

Figure 7. Thyroid dysfunction caused by overnutrition is reversible. Male mice were placed on the HF+SD for 6 weeks and then switched to the CD for 6 weeks (REV). BW was measured weekly (A). BAT, iWAT, and gWAT depots were weighed immediately after dissection (B). Terminal sera were analyzed by immunoassay for total T_3 (C). Plasma and sera were analyzed by immunoassay for total T_4 (D) and TSH (E). Some thyroids were weighed immediately upon dissection (F). Other thyroids were fully proteolyzed, and liberated T_4 (G) and T_3 (H) were then measured by immunoassay and normalized to the thyroidal protein. Other thyroids were fixed for H&E staining, and H&E images were then blindly scored for extent of interfollicular vascular/lymphatic space (I). Western blot of thyroid homogenate was performed for TG and quantitated (J). Data are representative of two separate cohorts of mice (A, B, G, H). *n* = 12-15/group (A), *n* = 15/group (D, E). Data were analyzed by 2-way ANOVA with multiple comparisons (A, D, E), unpaired Student's *t*-test with Welch's correction (B: WAT, C, F–J), or Mann-Whitney test (B: BAT). *$p < 0.05$, **$p < 0.01$, & ****$p < 0.0001$ vs. controls within that timepoint. #$p < 0.05$, ##$p < 0.01$, & ###$p < 0.001$ vs. week 0 within that diet group.

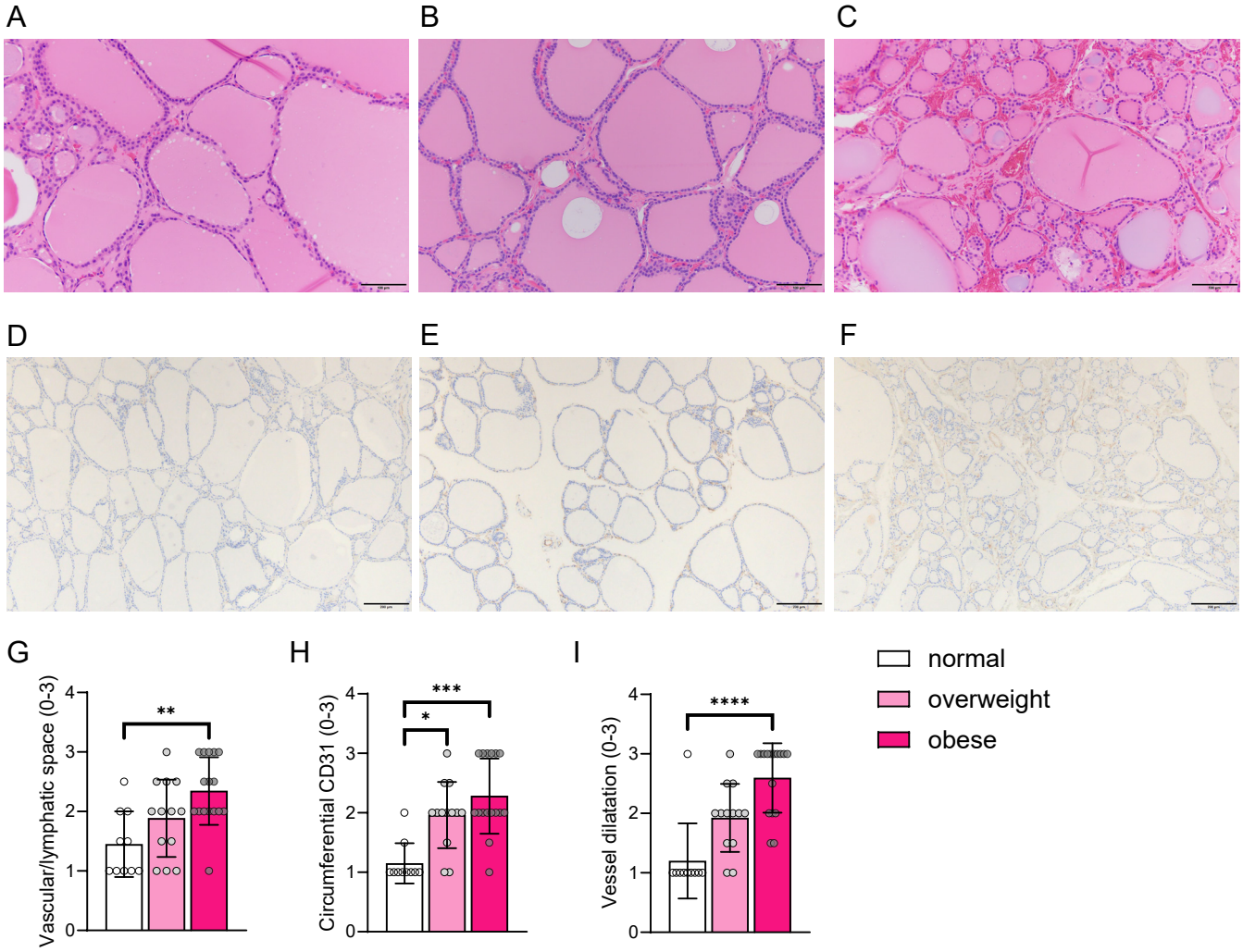

Figure 8. Thyroidal vascularization increases with increasing BMI in humans. H&E-stained sections of thyroid tissue from patients with multinodular goiter (MNG) were obtained. Representative images from normal (A), overweight (B), and obese (C) subjects are shown. Fixed thyroid sections were stained for vascular marker CD31, and representative images from normal (D), overweight (E), and obese (F) subjects are shown. H&E images were blindly scored for the extent of vascular/ lymphatic space (G). CD31 images were blindly scored for extent of circumferential staining around the follicles (H) and dilatation of the follicular microcapillaries (I). Scale bars = 100 μm (A–C) or 200 μm (D–F). Normal n = 10, overweight n = 13, obese n = 16. Data were analyzed by Kruskal-Wallis test with Dunn's multiple comparison test. *$p < 0.05$, **$p < 0.01$, ***$p < 0.001$, & ****$p < 0.0001$.

Table 1. TSH-responsive gene expression.

Gene	Log_2 FC	*p*-value
Slc5a5 (NIS)	3.1	1.4E-18
Tshr	1.7	1.2E-07
Tpo	2.3	4.7E-11
Duox2	0.8	0.001
Tg	0.6	0.01
Dio1	2.0	9.3E-17

Thyroids were processed for RNA sequencing, and differential gene expression analysis was performed. The log_2 fold change (FC) of TSH-responsive genes expressed in the HF+SD group vs. controls, alongside the adjusted *p*-values, are shown. CD $n = 3$, HF+SD $n = 4$.

Table 2. Top 10 most up- and downregulated gene sets using GO annotations.

GO Gene Set	NES
GOBP attachment of spindle microtubules to kinetochore	2.41
GOBP renal system vasculature development	2.31
GOBP glomerulus development	2.26
GOBP kinetochore organization	2.25
GOBP integrin mediated signaling pathway	2.25
GOMF microtubule motor activity	2.24
GOCC condensed chromosome centromeric region	2.23
GOBP regulation of endothelial cell differentiation	2.23
GOBP mitotic sister chromatid segregation	2.23
GOBP protein localization to condensed chromosome	2.22
GOBP mitochondrial respiratory chain complex assembly	-2.83
GOBP mitochondrial electron transport NADH to ubiquinone	-2.84
HP abnormality of the mitochondrion	-2.86
HP abnormal activity of mitochondrial respiratory chain	-2.87
GOCC NADH dehydrogenase complex	-2.88
GOCC contractile fiber	-2.90
GOCC ribosomal subunit	-2.90
GOMF structural constituent of ribosome	-2.92
GOCC inner mitochondrial membrane protein complex	-3.10
GOCC mitochondrial protein containing complex	-3.20

Thyroids were processed for RNA sequencing, and gene set enrichment analysis was performed using GO annotations. Gene sets were ranked by normalized enrichment score (NES) of the HF+SD group vs. controls. CD $n = 3$, HF+SD $n = 4$. All adjusted p-values < 0.0002.